THE UNIVERSITY OF MICHIGAN

ON NEAR ZONE ANTENNAS

by

R. F. Goodrich and R. E. Hiatt

June 1959

Report No. 2861-1-F

Final Report on Purchase Order
211-500-8668

Prepared for

GENERAL ELECTRIC COMPANY
DEFENSE ELECTRONICS DIVISION
SYRACUSE, NEW YORK

Engrs

UMR

1640

I

INTRODUCTION

Given a finite source distribution, say a circular aperture of radius a, we wish to find the behavior of the resulting field at some finite distance R_o from the source.
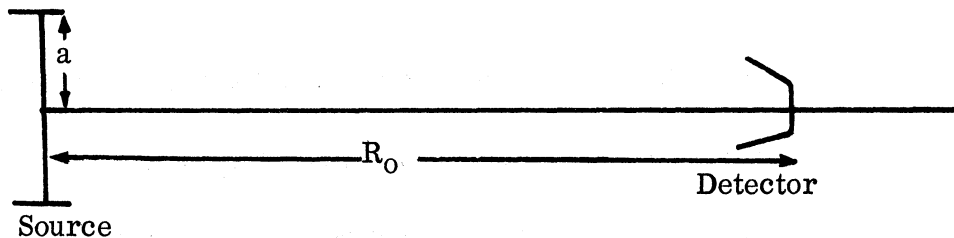

FIGURE I-1

We wish to determine the excitation which will lead to a focussing at R_o. More explicitly we wish to find the dependence of the strength of the field and the size of the focus on the parameters of the problem.

The focussing will obtain provided the phase of the excitation is proportional to the distance from a source element to the focus. The origin of this phase control of the excitation can be a phase controlled array or an elliptical reflector. In the latter case the source would be placed at one focus of the ellipse, the focussing will occur at the other focus of the ellipse.
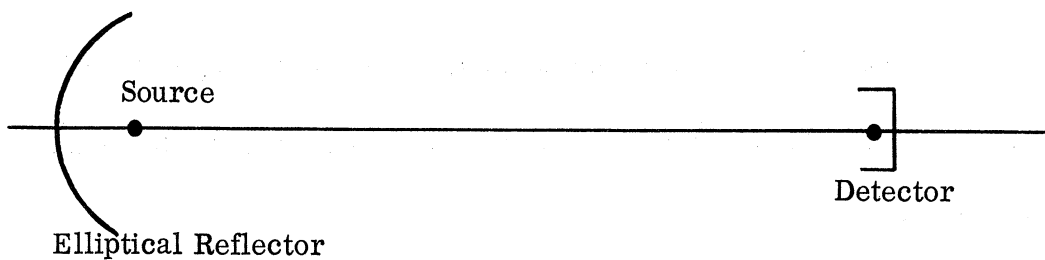
1

Source

Detector

Elliptical Reflector

FIGURE 1-2

Accepting this requirement on the phase distribution the problem is

then that of finding the dependence of the strength and spread of the field at

the focus on the amplitude of the distribution. To this end we deal with the

scalar problem. This is no essential restriction since we will be most

interested in the case in which the aperture size is considerably smaller than

the range, $a \ll R_o$. Under this assumption, $a \ll R_o$, the scalar and vector

problems are sensibly equivalent.

II

THE SCALAR PROBLEM

We consider a scalar source distribution $f(\rho)$ on an aperture of radius a.

The field due to this source is given by

$$\psi(\vec{R}) = \int \frac{e^{ik|\vec{R}-\vec{\rho}|}}{|\vec{R}-\vec{\rho}|} f(\vec{\rho}) \, dS \tag{2.1}$$

where R is the vector to the field point and ρ is the vector to the source point

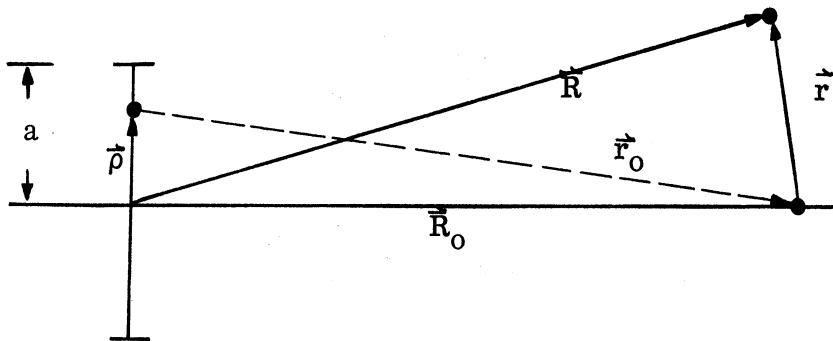with the origin at the center of the aperture as in Figure 2-1.

FIGURE 2-1

We now require the phase of the source distribution to be such that the field is

focussed at a point $\vec{R}_0$ on the axis. We put

$$f(\vec{\rho}) = e^{-ikr_0} g(\rho) \tag{2.2}$$

where $\vec{\rho} + \vec{R}_0 = \vec{r}_0$. Hence,

3

$$\psi(\vec{R}) = \int \frac{e^{ik|\vec{R}-\vec{\rho}|}}{|\vec{R}-\vec{\rho}|} \, e^{-ikr_0} \, g(\rho) \, dS \quad . \tag{2.3}$$

We now refer the field point to the point of focus and put

$$\vec{r} = \vec{R} - \vec{R}_0 \quad , \tag{2.4}$$

and take $R_0 \gg r$ and ρ. Making use of this inequality we use the approximation

$$\left|\vec{R}-\vec{\rho}\right| = R_0 \left\{ 1 - \frac{r \cdot \rho}{R_0^2} + \frac{1}{2} \frac{\rho^2}{R_0^2} - \frac{1}{2} \frac{r \cdot R_0}{R_0^4} \rho^2 + \cdots \right\} \tag{2.5}$$

and

$$r_0 = R_0 \left\{ 1 + \frac{1}{2} \frac{\rho^2}{R_0^2} \right\} + \cdots \quad . \tag{2.6}$$

Substituting, we have

$$\psi(\vec{r}) = \frac{1}{R_0} \int_S dS \, e^{-ik\left(\frac{r \cdot \rho}{R_0} + \frac{1}{2} \frac{r \cdot R_0}{R_0^3} \rho^2\right)} g(\rho) \tag{2.7}$$

where we use the approximation

$$\left|\vec{R}-\vec{\rho}\right| \cong R_0 \tag{2.8}$$

in the denominator but the higher order approximations, equations (2.5) and (2.6),

in the exponential. Further, we omit phase dependences independent of ρ .

We express the vectors, $\vec{\rho}$, $\vec{r}$, and $\vec{R}_0$ in the forms

$$\begin{cases} \vec{\rho} = \rho \, (\cos \emptyset, \, \sin \emptyset, \, 0) \\[2mm] \vec{r} = r \, (\sin \theta, \, 0, \, \cos \theta) \\[2mm] \vec{R}_0 = R_0 (0, \, 0, \, 1) \end{cases} \tag{2.9}$$

and equation (2.7) becomes

$$\psi(r) = \frac{1}{R_0} \int_0^a \rho \, d\rho \int_0^{2\pi} d\emptyset \; e^{-ik\left\{ \frac{r \, \rho \sin\theta}{R_0} \cos \emptyset + \frac{1}{2} \frac{r \cos\theta}{R_0^2} \rho^2 \right\}} \cdot g(\rho) \tag{2.10}$$

Under the assumption that the excitation $g(\rho)$ is independent of the angle $\emptyset$ the $\emptyset$-integration can be performed at once giving

$$\psi(r, \theta) = \frac{2\pi}{R_0} \int_0^a \rho \, d\rho \; e^{-\frac{ik}{2} \frac{r \cos\theta}{R_0^2} \rho^2} J_0\left(\frac{kr \sin\theta}{R_0} \rho \right) g(\rho) \tag{2.11}$$

where J_0 is the 0'th order Bessel function.

The problem is now to characterize the transformation of equation (2.11) leading from the excitation $g(\rho)$ to the field $\psi(r, \alpha)$. We start by considering the distribution $g(\rho)$ which will maximize $\left| \psi(0,0) \right|^2$ with the restriction that

$$\int_0^a \left| g(\rho) \right|^2 \rho \, d\rho = 1 \; . \tag{2.12}$$

5

Now

$$\psi(0,0) = \frac{2\pi}{R_0} \int_0^a \rho \, d\rho \, g(\rho) \ .$$

(2.13)

But by Schwartz' inequality

$$\left| \int_0^a \rho \, d\rho \, g(\rho) \right|^2 \leqslant \int_0^a |g|^2 \, \rho \, d\rho \cdot \int_0^a \rho \, d\rho \ ;$$

(2.14)

hence,

$$\left| \psi(0,0) \right|^2 \leqslant \left(\frac{2\pi}{R_0} \right)^2 \int_0^a \rho \, d\rho$$

(2.15)

where we note that the equality in (2.15) holds provided

$$g(\rho) \equiv \frac{\sqrt{2}}{a} \ .$$

(2.16)

Having shown that the uniform amplitude distribution leads to a "maximum gain" configuration we now investigate this case further. We deal with an integral of the form

$$I(\alpha, \beta) = \int_0^a x \, dx \, e^{-i \frac{\beta}{2} x^2} J_0(\alpha x) \ .$$

(2.17)

The integral of equation (2.17) is just a combination of Lommel functions of two variables (Ref. 1)

$$I(\alpha,\beta)= \frac{1}{\beta}\ e^{-\frac{i}{2}\beta a^2}\left[U_1(\beta,a^2,\ \alpha\ a)+i\ U_2(\beta,a^2,\ \alpha\ a)\right].$$ (2.18)

Putting this in the form of a Bessel function series of the Neumann type (Ref. 1)

we have

$$I(\alpha,\beta)= \frac{-i}{\beta}\ e^{-\frac{i}{2}\beta a^2}\ \sum_1^\infty\left(i\ \frac{\beta a}{\alpha}\right)^m\ J_m(\alpha\ a).$$ (2.19)

In our application of this representation to our problem we will require

the values of $I(\alpha,\beta)$ for $\alpha= 0$, $\beta= 0$, and $\alpha = \beta = 0$. These are

$$I(0,\beta)= -\frac{i}{\beta}\ e^{-\frac{i}{2}\beta a^2}\ \sum_1^\infty(i\beta a)^m\ \frac{\left(\frac{a}{2}\right)^m}{m!} = -\frac{i}{\beta}\ e^{-\frac{i}{2}\beta a^2}\left(e^{\frac{i}{2}\beta a^2} - 1\right)$$

$$= \frac{2}{\beta}\ e^{-\frac{i}{4}\beta a^2}\ \sin\left(\frac{\beta a^2}{4}\right)$$ (2.20)

$$I(\alpha,0)= \frac{a}{\alpha}\ J_1(\alpha\ a)$$ (2.21)

$$I(0,0)= \frac{a^2}{2}.$$ (2.22)

Returning to the representation of the field $\psi(r,\alpha)$ we have

$$\psi(r,\alpha)= -\frac{2\pi i}{R_0\beta}\ e^{-\frac{i}{2}\beta a^2}\ \sum_1^\infty\left(i\ \frac{\beta a}{\alpha}\right)^m\ J_m(\alpha\ a)$$ (2.23)

7

with

$$\alpha = \frac{kr \sin \theta}{R_o} \quad , \qquad \beta = \frac{kr \cos \theta}{R_o^2} \quad ;$$

hence,

$$\psi(r,\theta) = -2\pi i \frac{R_o}{kr \cos \theta} e^{-\frac{i}{2} \frac{kr \cos \theta}{R_o^2} a^2} \sum_1^\infty \left(i \frac{\cos \theta}{R_o \sin \theta} a\right)^m J_m\left(\frac{kr \sin \theta}{R_o} a\right) \qquad (2.24)$$

The special values are

$$\psi(r,0) = \frac{4\pi R_o}{kr} e^{-\frac{i}{4} \frac{kr a^2}{R_o^2}} \sin\left(\frac{kr a^2}{4R_o^2}\right) \qquad (2.25)$$

$$\psi(r,\frac{\pi}{2}) = \frac{2\pi a}{kr} J_1\left(\frac{kra}{R_o}\right) \qquad (2.26)$$

$$\psi(0,\theta) = \frac{\pi a^2}{R_o} \quad . \qquad (2.27)$$

We now investigate the zeros of ψ for the special values $\theta = 0$, $\pi/2$ of

its argument. First we consider r_1 such that

$$\psi(r_1, 0) = 0.$$

The first of these zeros occurs for

$$r_1 = \frac{4R_o^2}{ka^2} \pi = \frac{2\lambda R_o^2}{a^2} \quad . \qquad (2.28)$$

This indicates that for our assumption $a \ll R_0$ the first zero along the axis will occur many wavelengths from the focus $r = 0$.

For the second case $r = r_2$ such that

$$\psi \left(r_2, \frac{\pi}{2}\right) = 0,$$

the first zero occurs at

$$r_2 = \frac{R_0}{ka} j_1 = \frac{\lambda R_0}{2\pi a} j_1$$

where j_1 is the first zero of the first order Bessel function. Now $j_1 \cong 3.83$; hence

$$r_2 \cong \frac{3.83}{2\pi} \frac{R_0 \lambda}{a} \tag{2.29}$$

and the first zero occurs somewhat closer to the focus $r = 0$ than in the preceding case. This result, equation (2.29), indicates the limitation on the sharpness of the focus imposed by the physical parameters.

The form of equation (2.17) indicates that with no more difficulty we can develop the case of a Gaussian amplitude distribution. In fact, this simply involves taking the quantity β to be complex. We write

$$g(\rho) = e^{-\frac{\rho^2}{\mu^2}} \tag{2.30}$$

and put

$$\beta = \frac{kr \cos \theta}{R_0^2} - \frac{2i}{\mu^2} . \tag{2.31}$$

This complex β then leads to the following results for the special values

9

$\theta = 0$, $r = 0$:

$$\psi(r,0) = \frac{4\pi}{R_0} \; \frac{1}{\dfrac{kr}{R_0^2} - \dfrac{2i}{\mu^2}} \left(1 - e^{-\frac{ikr}{2R_0^2}a^2} \; e^{-\frac{\mu^2}{a^2}}\right) \tag{2.32}$$

$$\psi(0,\theta) = i \; \frac{\pi\mu^2}{R_0} \left(1 - e^{-\frac{\mu^2}{a^2}}\right) \quad . \tag{2.33}$$

We find that a certain approximate formulation will make the effect of the Gaussian excitation more transparent. We start with equation (2.17) as before and remark that for complex β as defined in equation (2.31) and for $\mu \gg a$ we can use the approximation

$$I(\alpha,\beta) \cong \int_0^\infty x \, dx \; e^{-i\frac{\beta}{2}x^2} \; J_0(\alpha x) \quad . \tag{2.34}$$

This integration can be performed in finite terms giving (Ref. 1)

$$I(\alpha,\beta) \cong -\frac{i}{\beta} \; e^{\frac{i\alpha^2}{2\beta}} \quad . \tag{2.35}$$

The transformation under this approximation takes a Gaussian into a Gaussian and we find

$$\psi(r,\theta) \cong -\frac{2\pi i}{R_0} \; \frac{1}{\dfrac{kr\cos\theta}{R_0^2} - \dfrac{2i}{\mu^2}} \; e^{i\frac{(kr)^3}{R_0^4} \frac{\cos\theta\sin^2\theta}{\left(\dfrac{kr\cos\theta}{R_0^2}\right)^2 + \dfrac{4}{\mu^4}}} \cdot e^{-\frac{2}{\mu^2}\left(\dfrac{kr\sin\theta}{R_0}\right)^2 \frac{1}{\left(\dfrac{kr\cos\theta}{R_0}\right)^2 + \dfrac{4}{\mu^4}}} \quad . \tag{2.36}$$

We now use equation (2.36) to approximate the case $\theta = \frac{\pi}{2}$. We have

$$\psi(r, \frac{\pi}{2}) \cong - \frac{\pi \mu^2}{R_0} \, e^{-\frac{1}{2} \left(\frac{kr}{R_0}\right)^2 \mu^2} . \qquad (2.37)$$

The use of the approximation in equation (2.34) for the Gaussian excitation while of no great interest to the central problem does illustrate the important result of this analysis. The behavior of the field as a function of the excitation is essentially the same as for the far field cases. A uniform amplitude gives a maximum gain configuration while a Gaussian amplitude gives a zero side-lobe configuration.

In conclusion, we see the restriction imposed on the focussing effect by the physical parameters may be summed up by equation (2.29).

III

PATTERN CALCULATIONS

We now turn to a more detailed consideration of the fields arising from

a uniform or Gaussian excitation of the aperture. To this end we will find it

convenient to express the fields in terms of cylindrical coordinates having their

origin at the focus and the z-axis along the axis of aperture as in Figure 3-1.
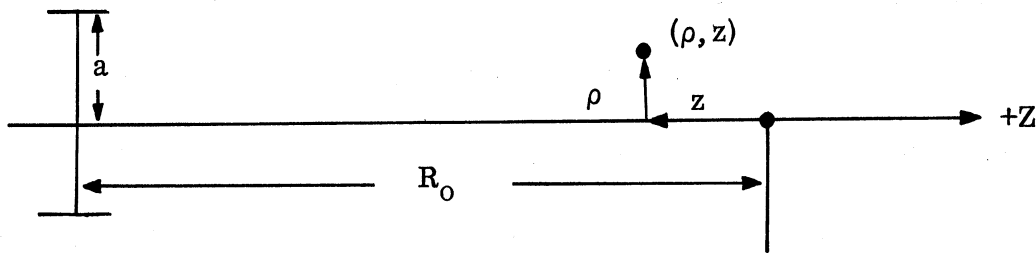

FIGURE 3-1

We will find that the field pattern is expressible as a linear combination

of tabulated basic patterns. More precisely, the field pattern is an infinite

series of these basic patterns the coefficients of which are given as powers of

certain "small" parameters.

We will truncate the series of basic patterns and compute various patterns

for the uniform amplitude configuration. Finally, we will compare the theoretical

results with those of a series of experiments using an elliptical reflector.

Recapitulating the previous section, we have

$$\psi = \frac{2\pi}{R_0} I(\alpha, \beta) \tag{3.1}$$

where

$$I(\alpha,\beta) = \frac{1}{\beta} e^{-i\beta a^2/2} \left\{ U_1(\beta a^2, \alpha a) + iU_2(\beta a^2, \alpha a) \right\}$$

$$= -\frac{i}{\beta} e^{-i\beta a^2/2} \sum_1^\infty \left(\frac{i\beta a^2}{\alpha} \right)^m J_m(\alpha a). \tag{3.2}$$

If we rewrite the series in terms of the function (Ref. 2, p. 128)

$$\Lambda_m(x) = (2/x)^m \, m! \, J_m(x), \tag{3.3}$$

equation (3.2) becomes

$$I(\alpha,\beta) = -\frac{1}{\beta} e^{-i\beta a^2/2} \sum_1^\infty \frac{[i(\beta/2) a^2]^m}{m!} \Lambda_m(\alpha a). \tag{3.4}$$

Recalling that for the Gaussian excitation

$$\begin{cases} \alpha = \dfrac{kr \sin \theta}{R_0} \\[4mm] \beta = \dfrac{kr \cos \theta}{R_0^2} - \dfrac{2i}{\mu^2} \end{cases} \tag{3.5}$$

we make the identification of the cylindrical coordinates

$$\begin{cases} z = r \cos \theta \\[2mm] \rho = r \sin \theta; \end{cases} \tag{3.6}$$

hence,

$$\begin{cases} \beta a^2 = kz \left(\dfrac{a}{R_0} \right)^2 - 2i \left(a/\mu \right)^2 \\ \\ \alpha a = k\rho \left(a/R_0 \right). \end{cases} \tag{3.7}$$

Now we have assumed $a \ll R_0$ and anticipating that the interesting Gaussian excitations will be relatively broad, i.e., $a \ll \mu$, we define the "small" parameters

$$\begin{cases} \eta \equiv a/R_0 \\ \\ \zeta = a/\mu \ . \end{cases} \tag{3.8}$$

Substituting in equation (3.1) we have an expansion explicitly exhibiting these "small" parameters,

$$\psi(\rho, z) = \frac{\pi a^2}{R_0} \frac{\exp\left[-\zeta^2 + (ikz/2)\, \eta^2 \right]}{\zeta^2 + (ikz/2)\, \eta^2} \sum_{1}^{\infty} \frac{\left[\zeta^2 + (ikz/2)\eta^2 \right]^m}{m!} \Lambda_m(k\rho\eta). \tag{3.9}$$

We now need to consider the properties of the functions $\Lambda_m(x)$. These are tabulated and graphed in Reference 2, pp. 180-189, so we restrict our consideration to a qualitative description. We take m as positive integer and $x \geq 0$.

Each of the $\Lambda_m(x)$ show a damped oscillatory behavior with a maximum at $x = 0$, $\Lambda_m(0) = 1$. This is illustrated in Figure 3-2 where we use $\Lambda_1(x)$ and $\Lambda_2(x)$ as prototypes.
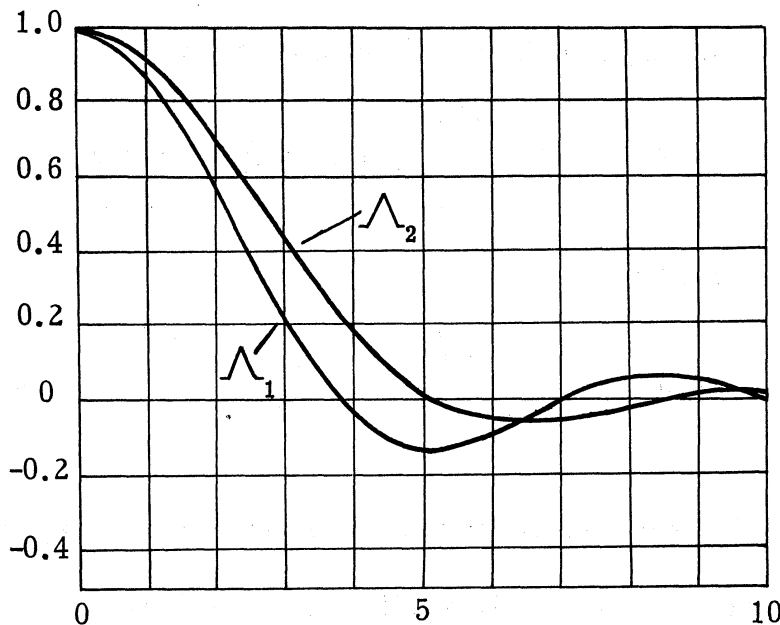

FIGURE 3-2

$\Lambda_1(x)$ and $\Lambda_2(x)$

As the order m increases the main lobe becomes broader. In fact, if we call $x_m \neq 0$ the first non-vanishing zero of the Bessel function $J_m(x)$, $J_m(x_m) = 0$, we have $x_m > x_{m-1}$ for all $m \geqslant 0$ and these values give a measure of the width of the main lobe.

We normalize the field to unit amplitude at $\rho = z = 0$, $\zeta = 0$, and split off the first term of the series

$$\underline{\psi}(\rho, z; \eta) = e^{-\zeta^2} \left\{ \Lambda_1(k\rho\eta) + \sum_1^\infty \frac{\left[\zeta^2 + (ikz/2)\eta^2 \right]^m}{(m+1)!} \Lambda_{m+1}(k\rho\eta) \right\}.$$

(3.10)

15

Now in the focal plane z = 0 and for a uniform amplitude excitation, $\zeta = 0$, the field is given by

$$\underline{\psi}_0 (\rho, 0) = \bigwedge_1 (k\rho \, \eta). \tag{3.11}$$

Hence, our expansion, equation (3.10), is of the form

$$\underline{\psi}(\rho, z; \zeta) = e^{-\zeta^2} \left\{ \underline{\psi}_0(\rho, 0) + \underline{\psi}' (\rho, z; \zeta) \right\} \tag{3.12}$$

where we have written $\underline{\psi}'$ for

$$\underline{\psi}'(\rho, z; \zeta) = \sum_1^{\infty} \frac{\left[\zeta^2 + (ikz/2) \, \eta^2 \right]^m}{(m+1)!} \bigwedge_{m+1} (k\rho \, \eta). \tag{3.13}$$

This term (3.13) is the correction to the focal plane pattern expressed as a series expansion in powers of the small parameters ζ and η .

For uniform illumination, $\zeta = 0$, and in the focal plane, z = 0 , the pattern is given by equation (3.11). Furthermore, as long as the requirements $\eta << 1$ and $\rho << R_0$ are met this single expression holds for these various values of the dimensions a and R_0.

Suppose we fix the wavelength and examine the behavior of the pattern as a function of the parameter η . If we take some criterion for the size of the region of focus, say the distance out to the half-power points, we can express the size of this spot as a function of η . For example, for the half-power criterion we have

$$\begin{cases} k\rho\,\eta \,\cong\, 1.6 \\ \\ \rho \,=\, \dfrac{0.8\lambda}{\pi}\,\dfrac{R_o}{a}\,. \end{cases} \tag{3.14}$$

More generally we can say that whatever our criterion, the size of the spot

is proportional to the range R_0.

As we move out of the focal plane, again for uniform amplitude in the

aperture, we note that for kz so small that only two terms of the series (3.10)

are required the energy in the pattern is given by

$$\left|\psi\right|^2 \,=\, \left|\Lambda_1\right|^2 + \left(\frac{kz\,\eta^2}{4}\right)^2 \left|\Lambda_2\right|^2 \,, \tag{3.15}$$

where we note that to this order the pattern is symmetric in z up to the inverse

square dependence on the distance from the source.

We will give examples of the uniform amplitude patterns for various

values of z and η . We will find it convenient to re-define our parameters

somewhat. We write

$$\begin{cases} R_o \,=\, a^2/M\lambda\,, \\ \\ z \,=\, \epsilon R_o,\, \left|\epsilon\right| \,<<\, 1. \end{cases} \tag{3.16}$$

The arguments of the field function then become

$$\begin{cases} \dfrac{kz}{2}\,\eta^2 \,=\, \pi\epsilon\,M \\ \\ k\rho\,\eta \,=\, 2\pi\,M\,\dfrac{\rho}{a}\,. \end{cases} \tag{3.17}$$

We substitute the expressions (3.17) in equation (3.10) for $\zeta = 0$

$$\underline{\psi}(\rho,z;0) = \bigwedge\nolimits_1 (2\pi M \tfrac{\rho}{a}) + \sum_1^{\infty} \frac{(\pi \epsilon M)^m}{(m+1)!} \bigwedge\nolimits_{m+1}(2\pi M \tfrac{\rho}{a}). \tag{3.18}$$

Including the first two terms and explicitly introducing the dependence on the

distance from the source we have the pattern function

$$f(\rho, \epsilon) = \left| \frac{\underline{\psi}(\rho,z;0)}{1+\epsilon} \right|^2 \tag{3.19}$$

$$= \frac{1}{(1+\epsilon)^2}\left[\left| \bigwedge\nolimits_1 (2\pi M \tfrac{\rho}{a}) \right|^2 + (\pi\epsilon M/2)^2 \left| \bigwedge\nolimits_2 (2\pi M \tfrac{\rho}{a}) \right|^2 \right]$$

where

$$\begin{cases} \epsilon = z/R_o, \quad |\epsilon| \ll 1 \\ \\ M = a^2/R_o \lambda \quad . \end{cases} \tag{3.20}$$

We plot $f(\rho, \epsilon)$ in db below $f(0,0) = 1$ in Figures 3-3, 3-4, 3-5, and 3-6 for

the values

$$M = 1.2; \qquad \epsilon = 0, \pm 0.12, \pm 0.24$$

$$M = 0.5; \qquad \epsilon = 0, \pm 0.10, \pm 0.25 \tag{3.21}$$

$$M = 0.1; \qquad \epsilon = 0, \pm 0.10, \pm 0.25.$$

$$\epsilon = 0; \qquad M = 1.2, \quad 0.5, \quad 0.1.$$
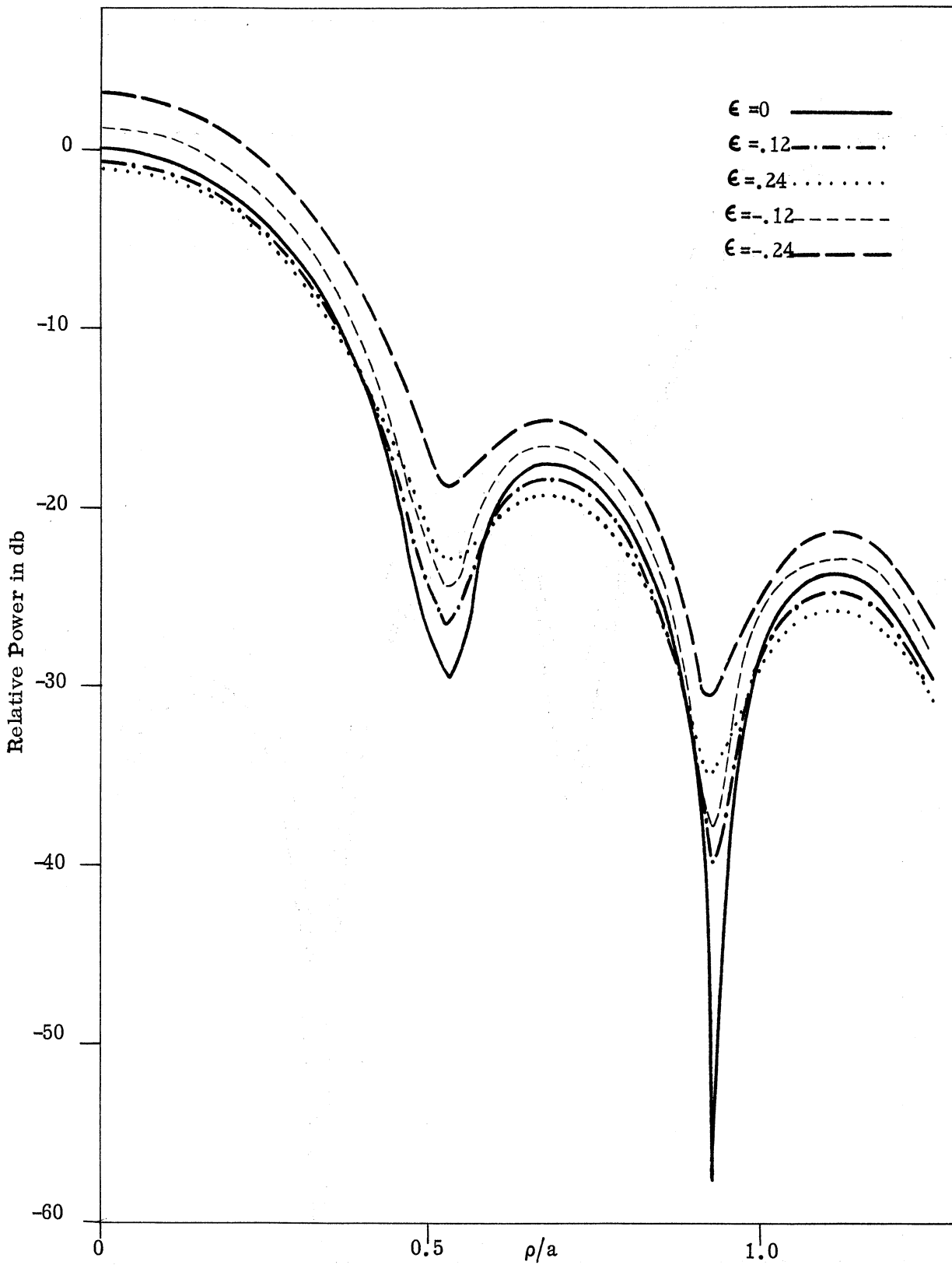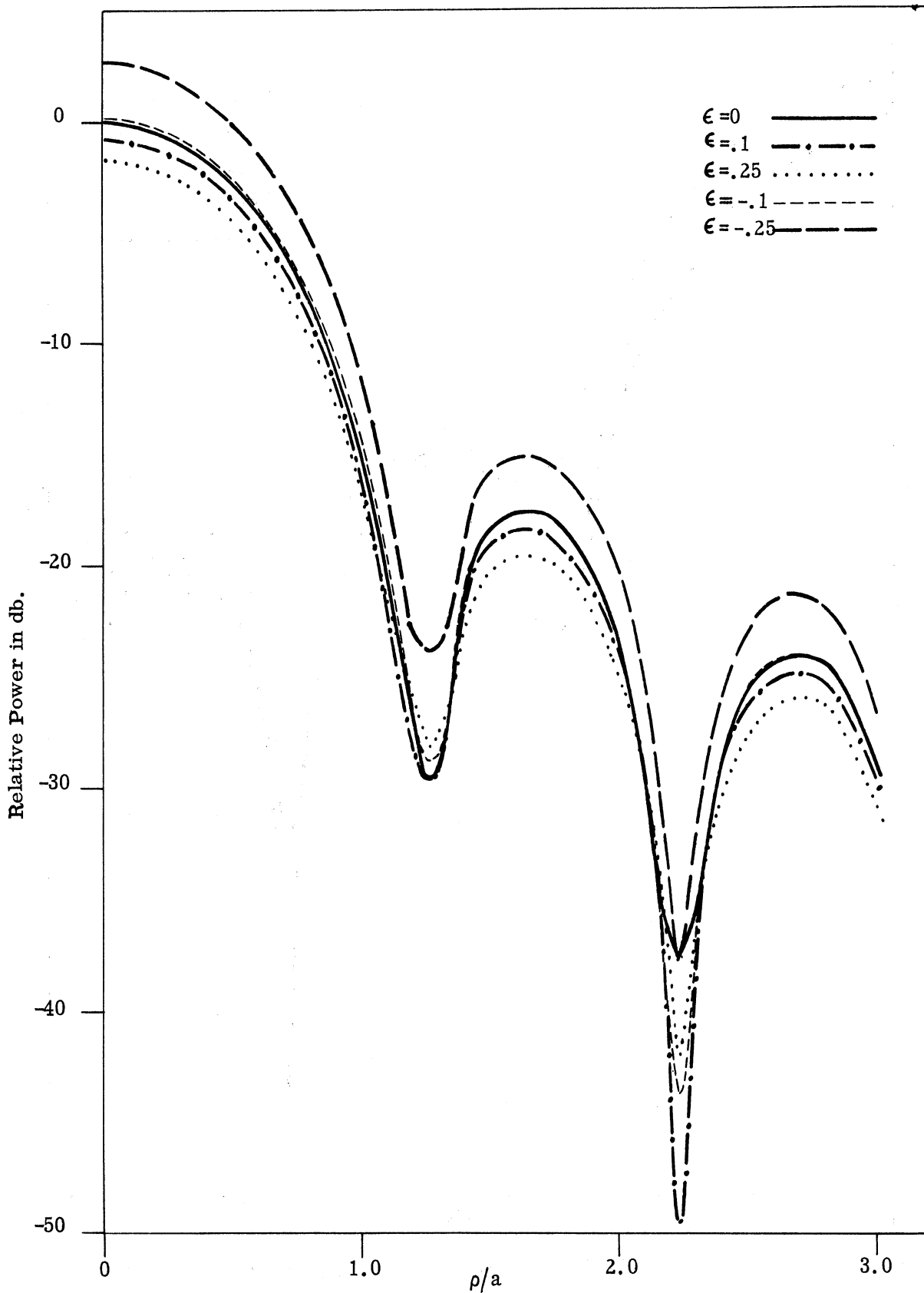
FIG. 3-3: f(ρ,ϵ) VS. ρ/a FOR M = 1.2

FIG. 3-4: $f(\rho, \epsilon)$ VS. ρ/a FOR M = 0.5

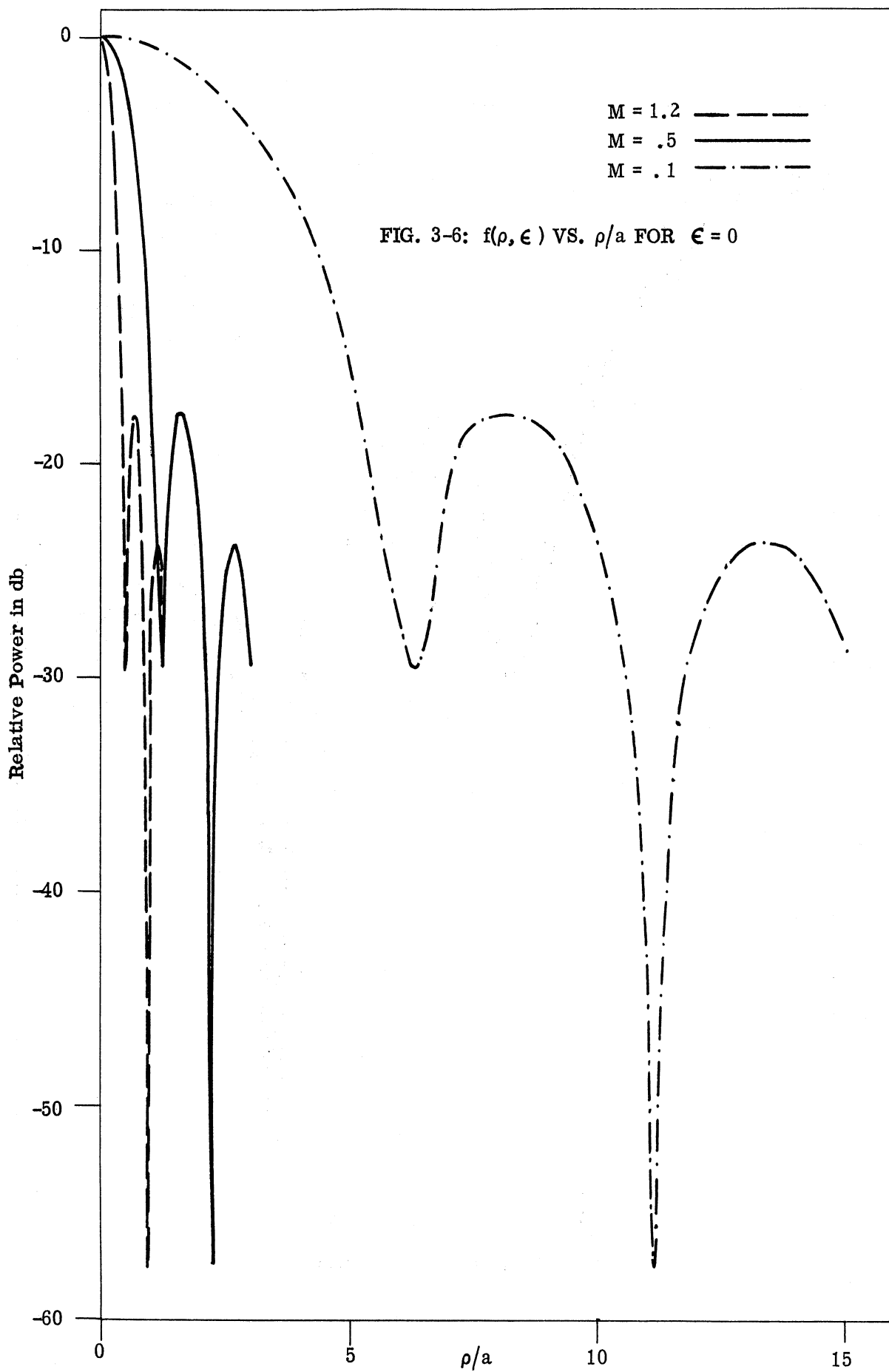FIG. 3-5: $f(\rho,\epsilon)$ VS. ρ/a FOR M = 0.1

FIG. 3-6: $f(\rho, \epsilon)$ VS. ρ/a FOR $\epsilon = 0$

M = 1.2
M = .5
M = .1

Relative Power in db

ρ/a
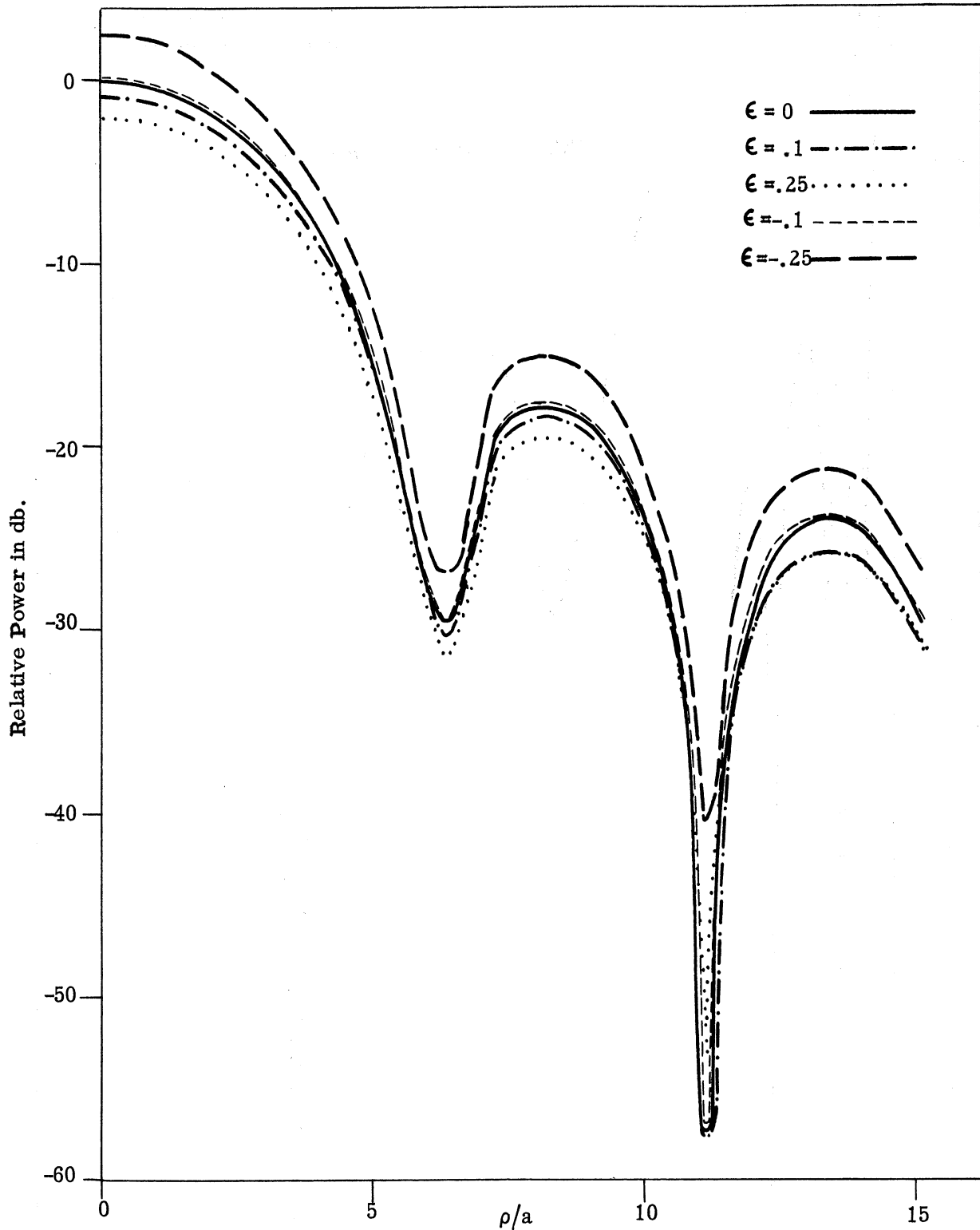
Finally, we will make a comparison with certain of the experiments described in Section IV which follows. We consider the H plane pattern using the modified waveguide feed. Now in the experiment the aperture illumination is tapered to a value 6 db below the center. This implies for the field a reduction of one-half at the edge of the aperture. Hence we take $\zeta^2 = 0.7$ and compute the pattern using equation (3.10). The other necessary parameter appears in the first case of the uniform amplitude pattern calculations, M= 1.2.

From equation (3.10) we have

$$\underline{\psi}(0,0;\ ) = e^{-\zeta^2} \ \frac{e^{\zeta^2} - 1}{\zeta^2}$$

$$= e^{-(\zeta/2)^2} \ (2/\zeta^2) \sinh (\zeta^2/2). \tag{3.22}$$

Hence, in order to normalize to unity at $z = \rho = 0$ we write, including the dependence on the distance from the source, the pattern function

$$f(\rho, \epsilon\ ;\zeta) = \left| \frac{\underline{\psi}(\rho,\ z;\zeta)}{(1+\epsilon)\ \underline{\psi}(0,\ 0;\zeta)} \right|^2 \tag{3.23}$$

Because of the size of $\zeta^2 = 0.7$ we include three terms in truncating the series and write

$$f(\rho,\epsilon\ ;\zeta) = \frac{1}{(1+\epsilon)^2} \left(\frac{\zeta^2}{e^{\zeta^2}-1} \right)^2 \left\{ \left[\bigwedge_1 (2\pi\ M\ \frac{\rho}{a}) + \frac{\zeta^2}{2} \bigwedge_2 + \frac{\zeta^4}{6} \bigwedge_3 - \frac{\pi^2\epsilon^2 M^2}{6} \bigwedge_3 \right]^2 \right.$$

$$\left. + \left[\frac{\pi\epsilon M}{2} \bigwedge_2 + \frac{\zeta^2 \pi\epsilon M}{3} \bigwedge_3 \right]^2 \right\} \tag{3.24}$$

This expression (3.24) we compare with the experimental results in Figures
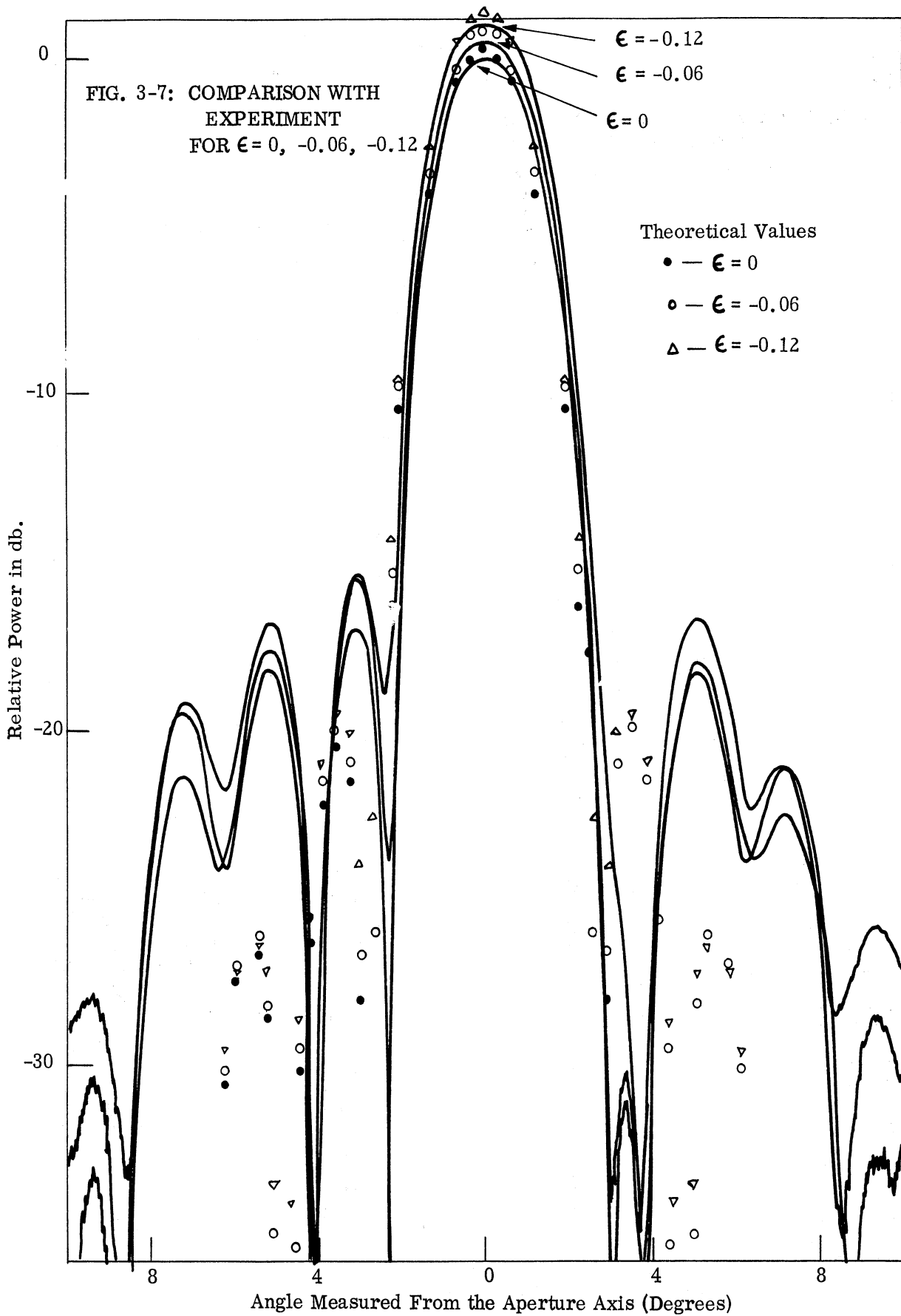
3-7 and 3-8 for the values
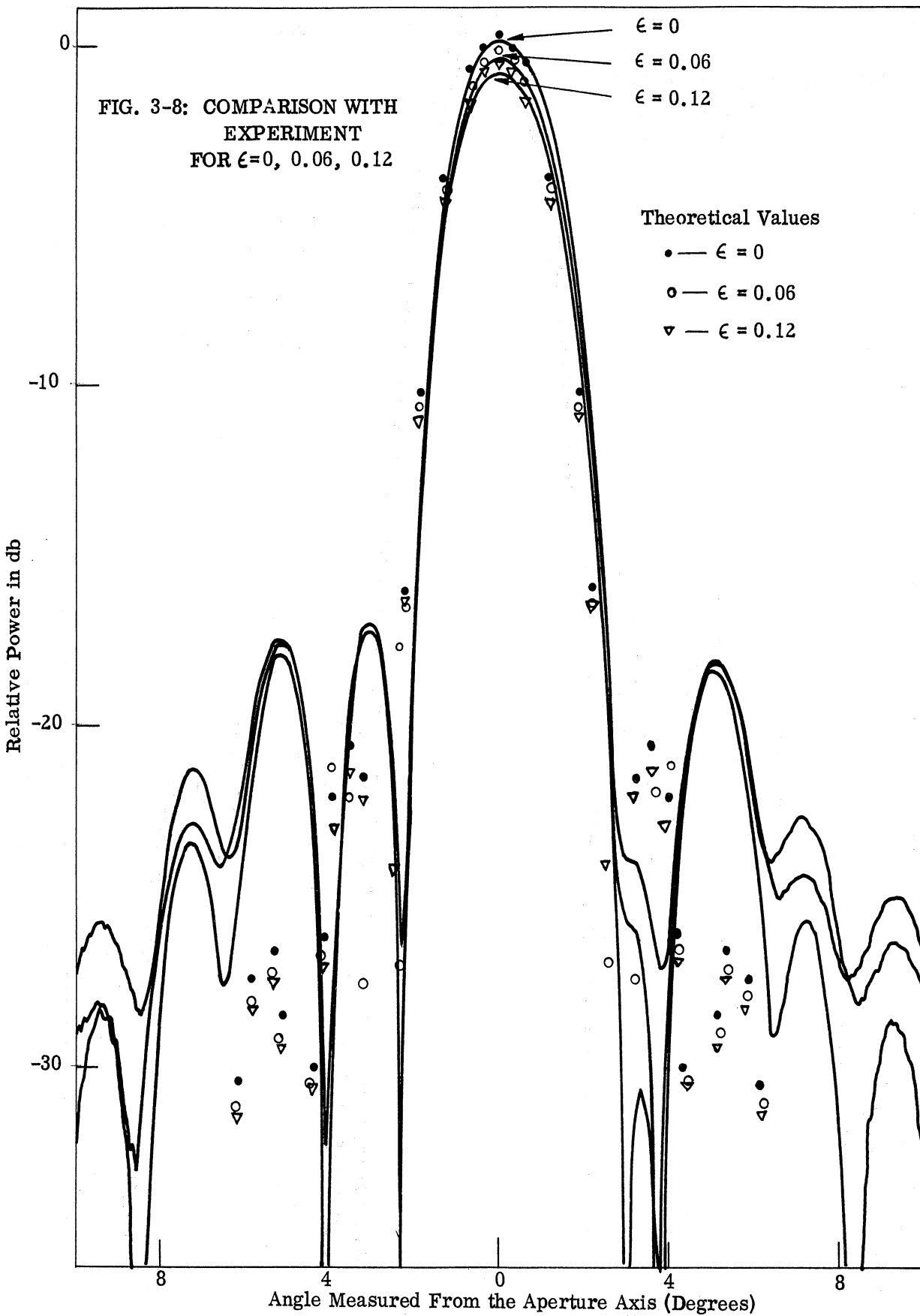
$$\epsilon = 0, \ \pm 0.06, \ \pm 0.12$$

The comparison with the experimental results in Figures 3-7 and 3-8

indicates that we can predict at least the main lobe whenever the aperture

illumination is able to be approximated by a Gaussian distribution. That this

form of the aperture illumination is not an essential restriction follows from

the fact that an arbitrary distribution is expressible as a series of Gaussians.

That is, we can expand a general aperture function $g(\rho)$ in a series,

$$g(\rho) = \sum_n a_n e^{-\rho^2/\mu_n^2} \tag{3.25}$$

This then leads to the field as a series of terms of the form of equation (3.10).

In closing we mention an extensive study of microwave lenses and image

formation by G. Bekefi (Ref. 4). This work was brought to our attention as this

report was being written. It considers in great detail the properties of the

image formed by a uniformly illuminated lens or aperture taking into account

the various optical aberrations.

FIG. 3-7: COMPARISON WITH
EXPERIMENT
FOR $\epsilon = 0$, -0.06, -0.12

$\epsilon = -0.12$

$\epsilon = -0.06$

$\epsilon = 0$

Theoretical Values

● — $\epsilon = 0$

○ — $\epsilon = -0.06$

△ — $\epsilon = -0.12$

Relative Power in db.

Angle Measured From the Aperture Axis (Degrees)

FIG. 3-8: COMPARISON WITH EXPERIMENT FOR ϵ = 0, 0.06, 0.12

IV

EXPERIMENTAL NEAR ZONE FOCUSSING OF PARABOLOIDAL AND PROLATE SPHEROIDAL DISHES

It is of interest to study experimentally the extent to which electromagnetic energy may be focussed to a point at some finite distance R_o from a circular aperture. As suggested in the introduction, the proper phase distribution to produce focussing is provided in an elliptical reflector. By placing the antenna feed at one focus of such a reflector, energy may be focussed to the other focal point. The degree to which this can be accomplished is dependent on how nearly the feed approximates a point source as well as upon the considerations discussed in the preceding sections.

The elliptical reflector chosen to study this phenomena was one whose surface is generated by revolving an ellipse about its major axis. The generating ellipse has a semi-major axis, 2a, of 225 inches and a semi-minor axis, 2b, of 90 inches. The reflector section consisted of the end cap extending to the first latus rectum. This gives an aperture of 36 inches; due to its rolled edges, the reflector procured had an aperture of about 35 inches. Focal point, f_1 of the reflector is approximately 9.4 inches from the vertex. The distance between focal points

$$R_o = 2(a^2 - b^2)^{1/2} = \sim 17.2 \text{ feet.}$$

To provide a basis of comparison, a second reflector type antenna was

also studied. The reflector used was a standard parabolic reflector, 35 inches

in diameter and with a focal length of 9 inches.

The feed used for these reflectors was a modified waveguide feed. The

modification, made as described in Silver (Ref. 3) produced a broader primary

pattern in the H plane than is achieved with a standard waveguide. Figure 4-2a

shows the E and H plane patterns of the feed. Since energy striking the edge of

the reflector travels two times as far as energy going to the reflector center, the

illumination taper is increased by 6 db making it about 12.5 db in the E plane and

about 13.2 db in the H plane.
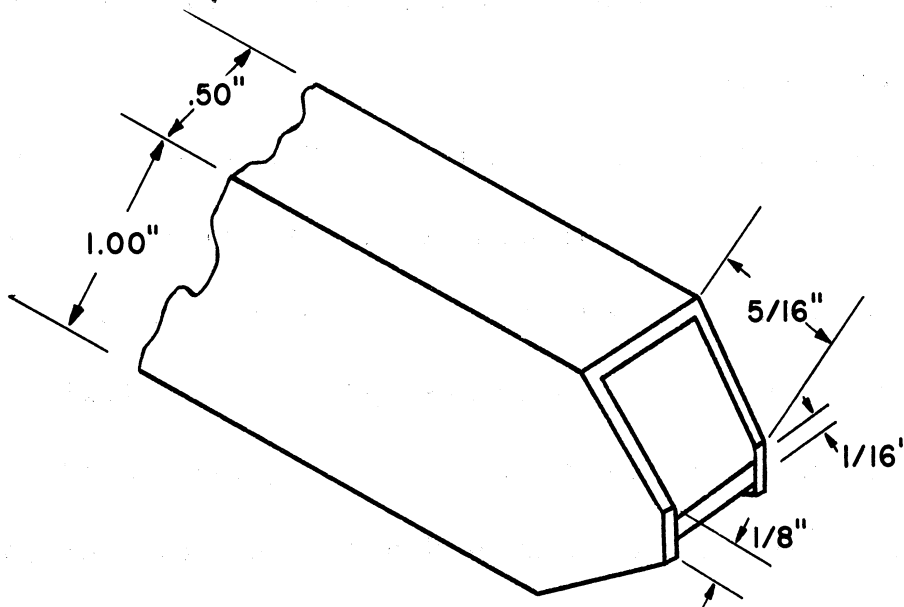
WAVEGUIDE (Reference 3, p. 381)

The location of the center of radiation of this feed was studied by exam-

ining the phase of the radiated energy. The results showed the center of phase

to be inside the waveguide. In the E plane the phase center was .16 λ from the

pin; in the H plane the phase center was .4λ from the pin. The phase, measured

on circles whose centers were at these points, was uniform to better than $\pm \lambda/16$

in both the E and H plane over the semi-circle occupied by the reflector.

In the last set of patterns presented (Fig. 4-9 and 4-10), a dipole feed,

fed by a coaxial line, was used to study the effect of a more uniform illumination.

Only H plane patterns were taken. In this case, the illumination taper at the edges

was down only 6 db and this was due to the factor of two difference in distance to

the center and to the edges of the dish.

All measurements were made at a frequency of 9450 mcs (λ = 1.25 inches).

The measurements were made in an indoor antenna range, some in a room 30 x 80

feet and others in the microwave free space room which is 30 x 60 feet. A photo-

graph of the free space room and of some of the equipment used is shown in Figure

4-1.

Both reflectors were first "checked out" as standard far-zone antennas.

Resulting E and H patterns are shown in Figure 4-2b. In these and in succeeding

patterns shown, the feed is positioned in the E and H plane to produce the optimum

patterns. As would be expected, these positions differ by 0.3 or 0.4 inches, due

to the difference in the effective center of radiation.

In studying the near zone behavior, the antenna under test served as the

receiver. It was mounted on an antenna pedestal which provided for rotation in

azimuth. A simple open waveguide was used as the transmitting antenna in order to provide as much detail as possible in the area being probed. This antenna and a stable X-band oscillator were mounted on a trolley which permitted the range to be varied over a fourteen-feet distance. This track was carefully aligned with the axis of the test antenna, so that peak signal was obtained at the same angular position of the test antenna as the transmitter was positioned at various points along the track.

A series of thirteen patterns were taken for eight conditions of the test antenna. The thirteen patterns were taken as the range was varied from R_0 (17.2 feet) to R_0 - 6 feet and R_0 + 6 feet in steps of one foot. For the reflectors used, this represents a change in range from .14 D^2/λ to 0.28 D^2/λ.

The first four sets of these patterns (Figures 4-3, 4-4, 4-5 and 4-6) are for the parabolic reflector. Figures 4-3 and 4-4 (E and H plane) show that a standard reflector, focussed for far-zone performance, is a very poor antenna for use at such short ranges. Figures 4-5 and 4-6 (E and H plane) show that it is possible to defocus the feed in a parabola so that a very acceptable beam is produced, even at .21 D^2/λ.

The patterns of the elliptical reflector are shown in Figures 4-7 through 4-10; the first two sets use the waveguide feed while the last two use the dipole feed. In Figure 4-10, the expanded angle scale is used to present more detailed information on the behavior in the focal region.

Summary curves showing 10 db and 3 db beamwidths of the patterns of

the parabolic and elliptical reflector are given in Figures 4-11 through 4-14.

Figure 4-15 is a plot of the received power vs range as the transmitting

antenna was pulled toward the receiver. The signal was first recorded on

the pattern recorder and later condensed and replotted as shown.

The agreement between predicted performance and experimental results

has been discussed in the preceding sections. It may be of interest to note

further that the beamwidths for both the defocussed parabola and the elliptical

reflector at the $0.21 \ D^2/\lambda$ range is approximately equal to or less than that

expected from a far field pattern of a uniformly illuminated parabola. The

patterns with the waveguide feed show beamwidths to be wider in the H plane

than in the E plane as would be expected due to the increased illumination taper

in the H plane. The sharpest patterns are obtained when the dipole is used as

a feed. These, of course, occur in the H plane where the illumination was

uniform except for the inverse distance squared loss.

The comparison between the linear width of the beam for the far field

and for the near field case is more striking. For the 35 inch elliptical reflector,

this width $(2R \tan \theta/2)$ is 7.5 inches as contrasted to the width of 37.6 inches

for the parabola when $R = D^2/\lambda$.

Table 4-1 compares the minimum beamwidths obtained experimentally

with theoretical values.[+]

[+]Reference 3 , p. 195.

TABLE 4-1

	Theoretical With Uniform Illumination 1.02 λ/D R = ∞	Experimental		
		Parabola Focussed For Far Field R = D^2/λ	Parabola Focussed For .21 D^2/λ	Elliptical Reflector R= .21D^2/λ
θ Beamwidth in Degrees	2.09	2.2	2.18	2.08
Beamwidth in Inches 2R tan θ/2	---	37.6	7.9	7.5

The gain of the parabolic and elliptical reflector antenna was measured at the range, R_o = 17.2 feet. With the modified waveguide feed in use in both antennas, the gain, measured by comparison with a gain standard, was 32.3 db for the parabola and 33.3 db for the elliptical reflector.
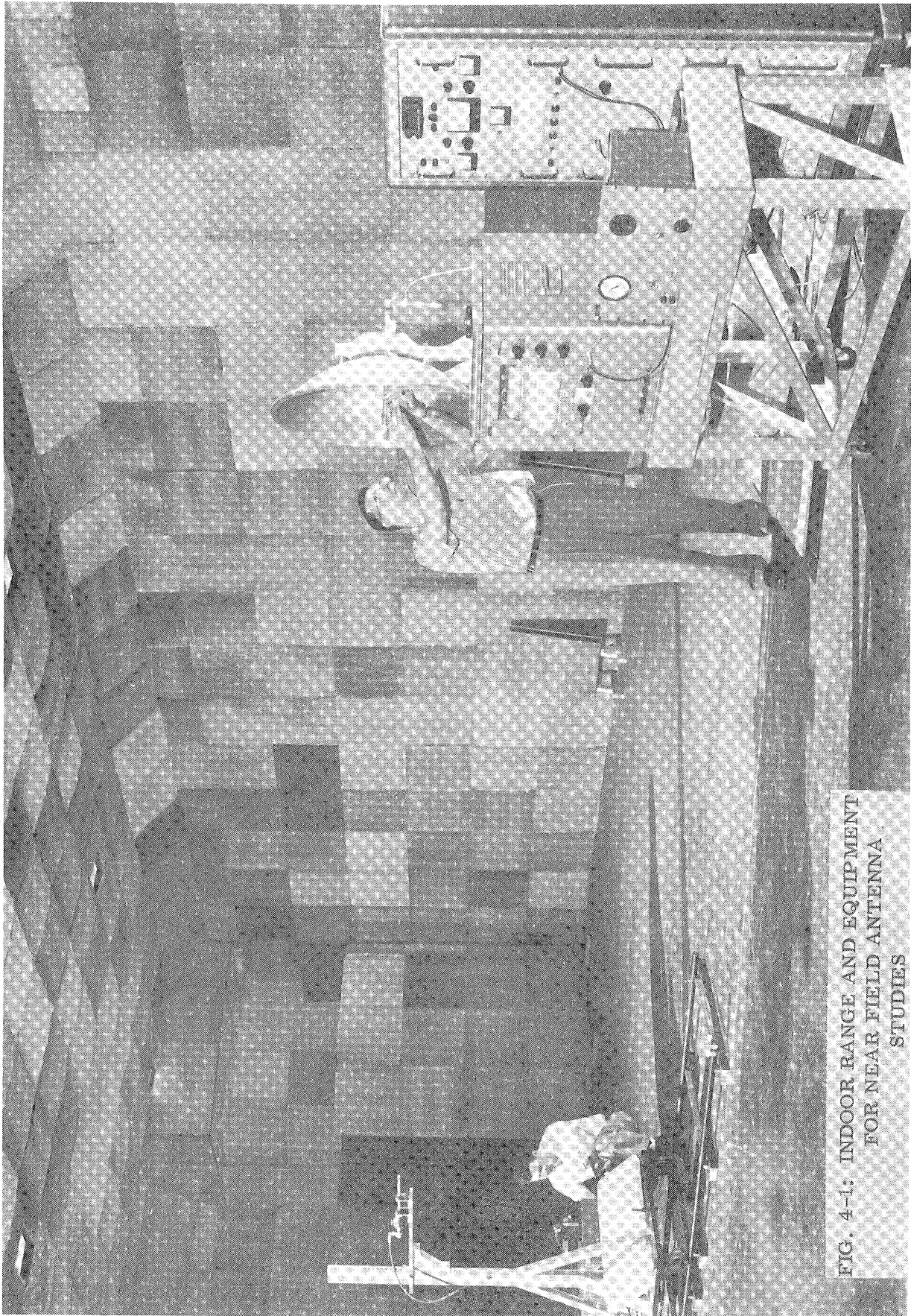
FIG. 4-1: INDOOR RANGE AND EQUIPMENT FOR NEAR FIELD ANTENNA STUDIES
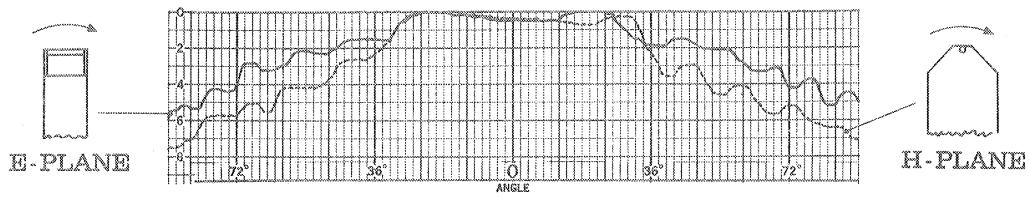
FIG. 4.2a: PRIMARY PATTERNS OF WAVEGUIDE FEED
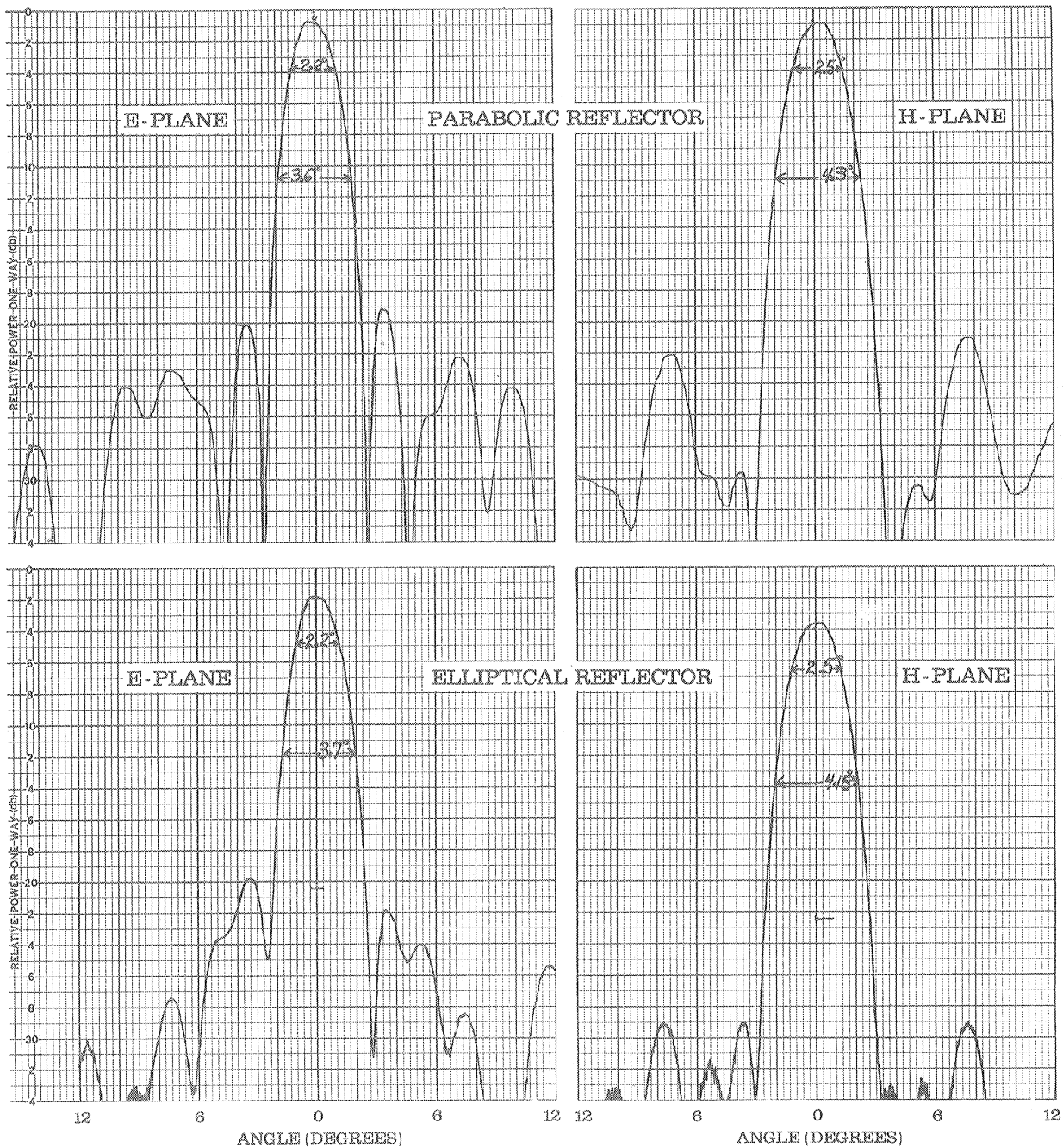
FIG. 4.2b: FAR FIELD PATTERNS
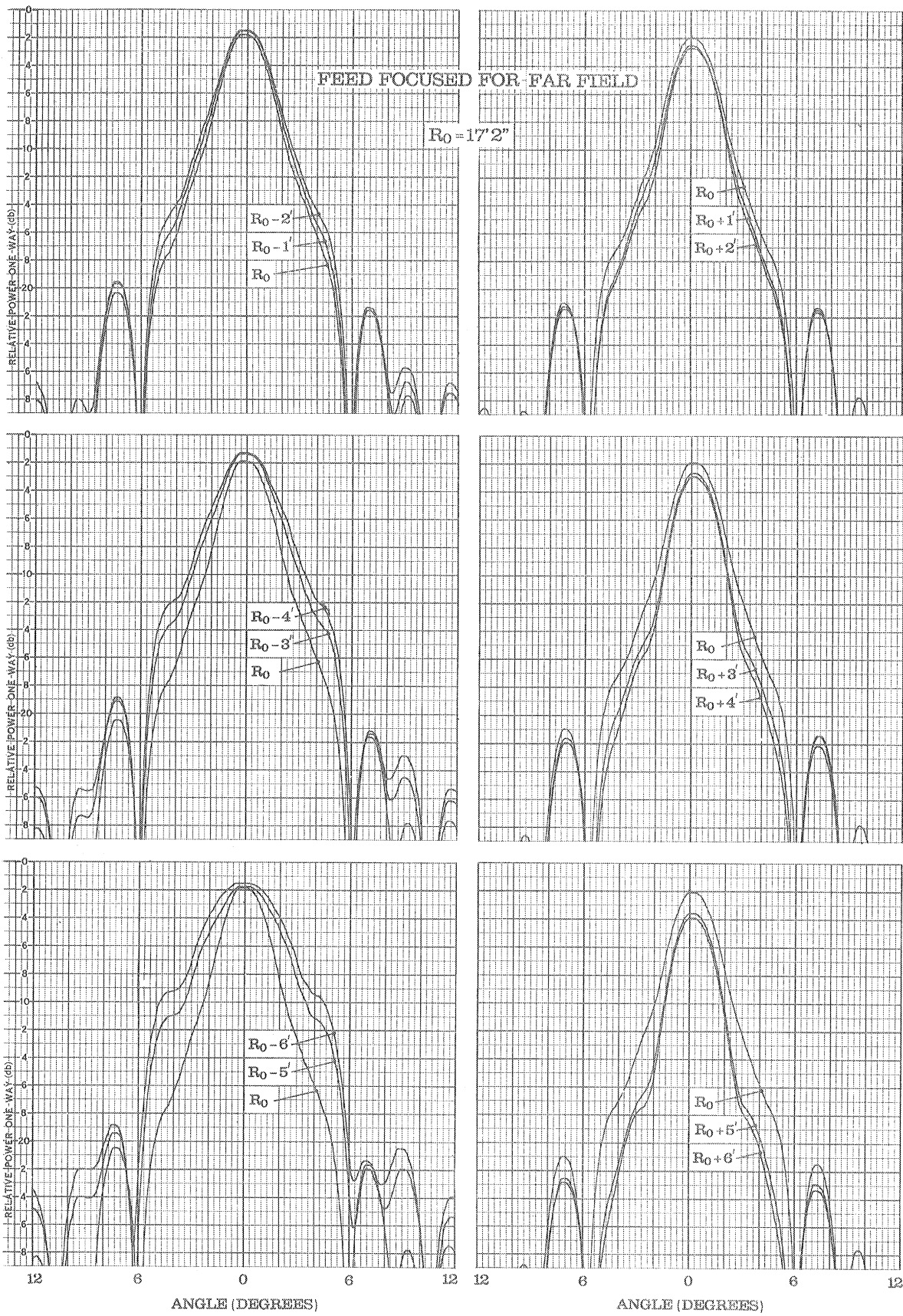
FIG. 4.3: E-PLANE NEAR FIELD PATTERNS OF PARABOLIC REFLECTOR
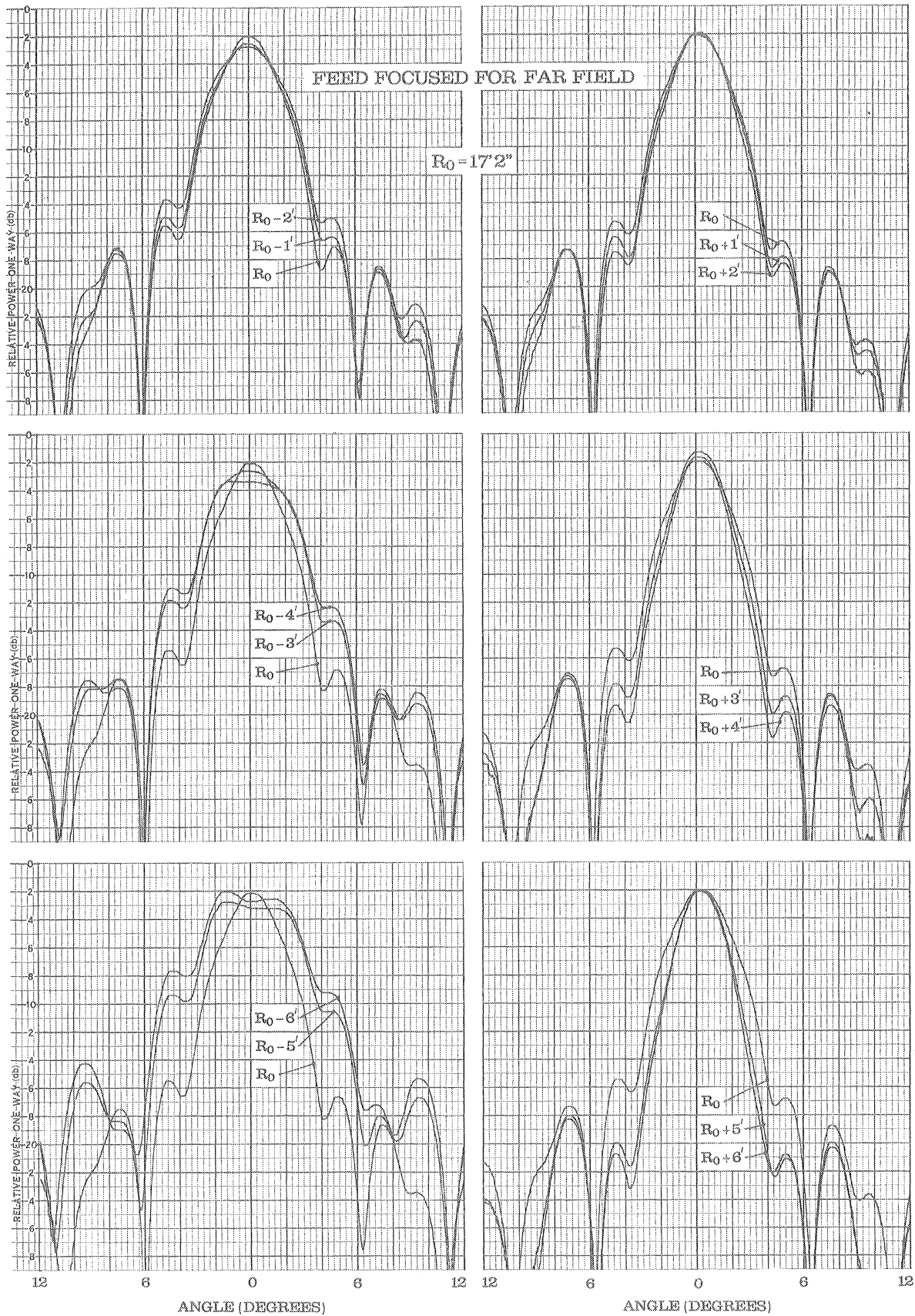
FIG. 4.4: H-PLANE NEAR FIELD PATTERNS OF PARABOLIC REFLECTOR
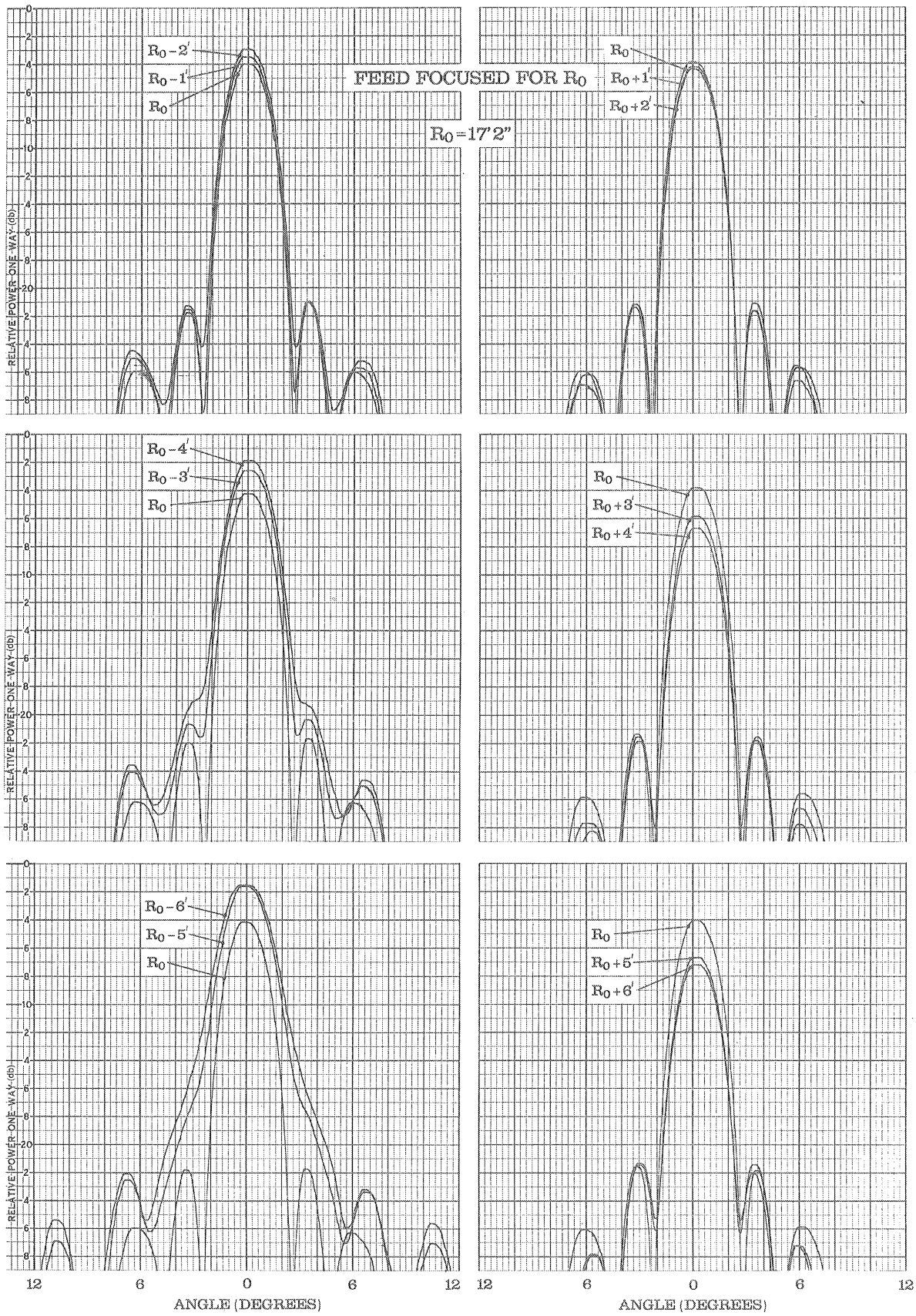
FIG. 4.5: E-PLANE NEAR FIELD PATTERNS OF PARABOLIC REFLECTOR, FOCUSED FOR R_0

FEED FOCUSED FOR R_0

$R_0 = 17'2''$

FIG. 4-6: H-PLANE NEAR FIELD PATTERNS OF PARABOLIC REFLECTOR,
FOCUSED FOR R_0

FEED FOCUSED FOR R_0

$R_0 = 17'2''$

WAVEGUIDE FEED
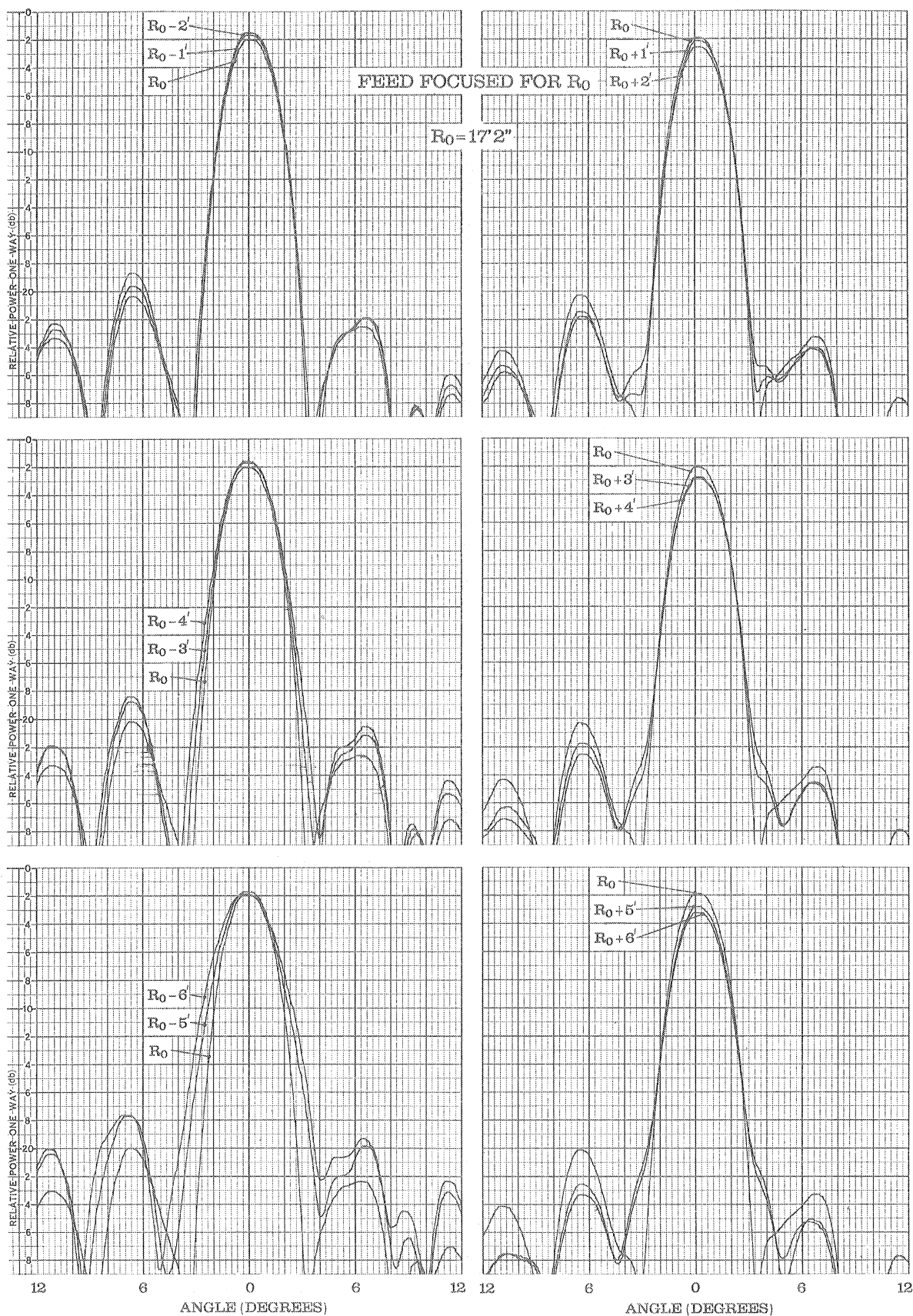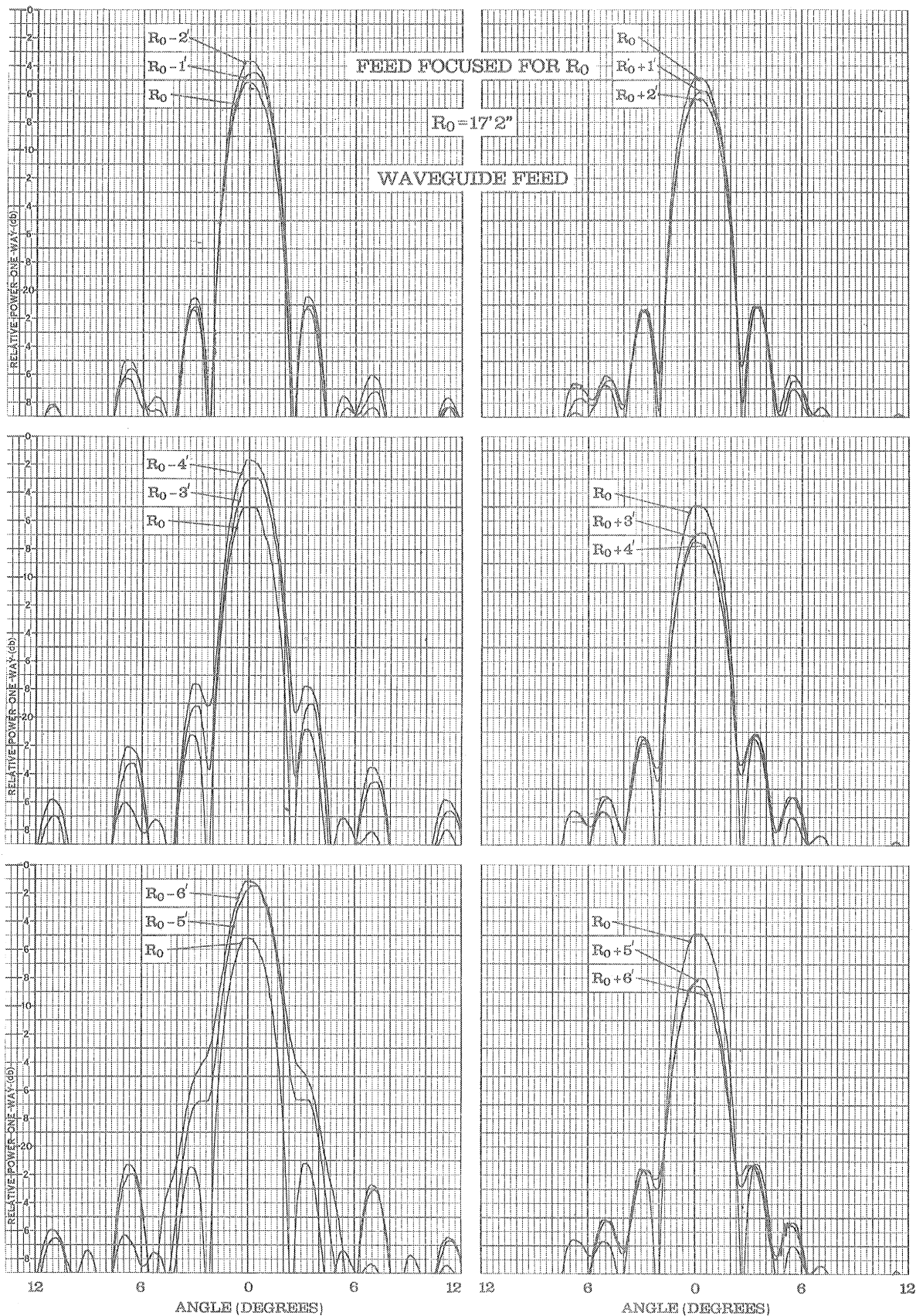
FIG. 4.7: E-PLANE NEAR FIELD PATTERNS OF ELLIPTICAL REFLECTOR
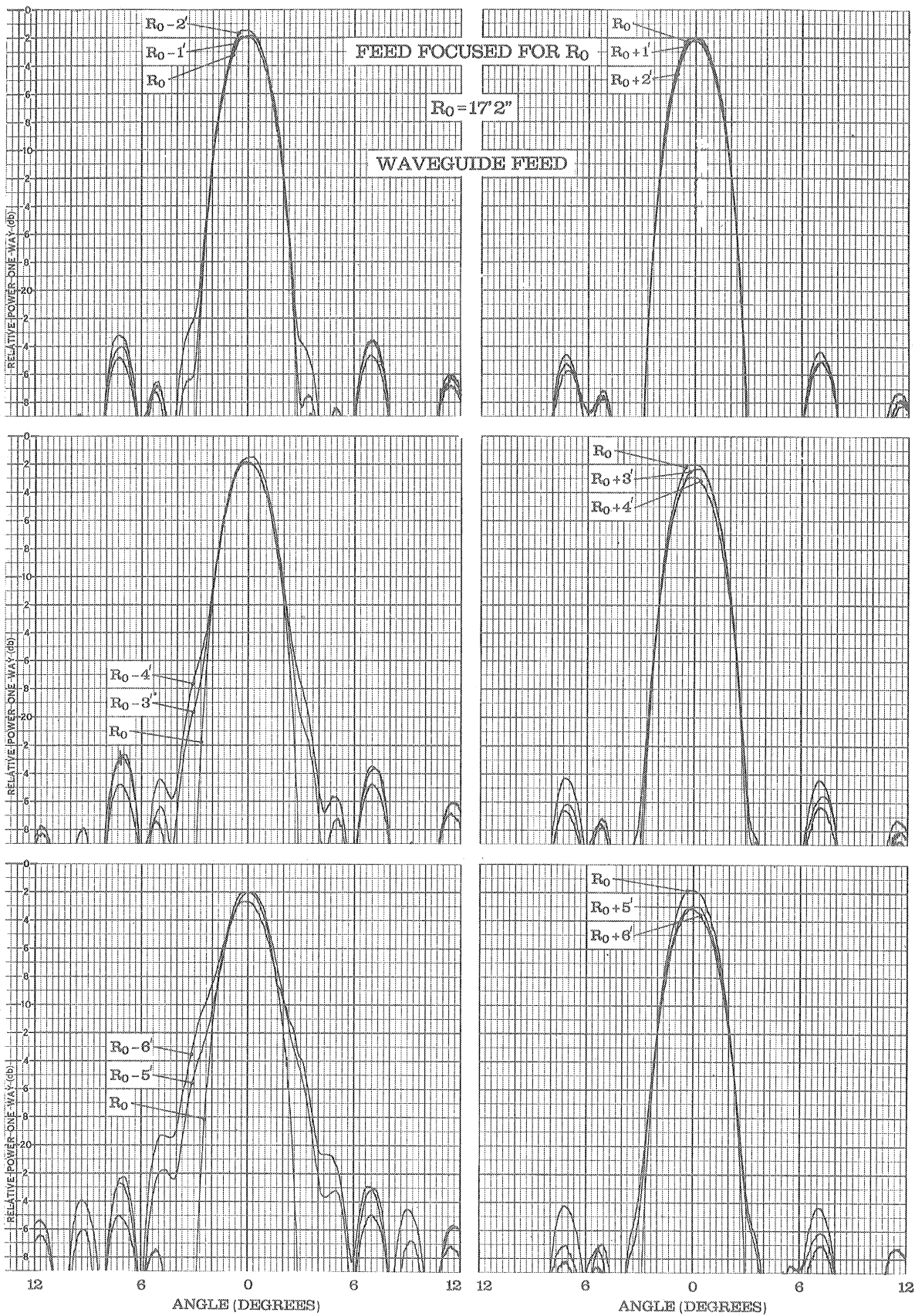
FIG. 4.8: H-PLANE NEAR FIELD PATTERNS OF ELLIPTICAL REFLECTOR
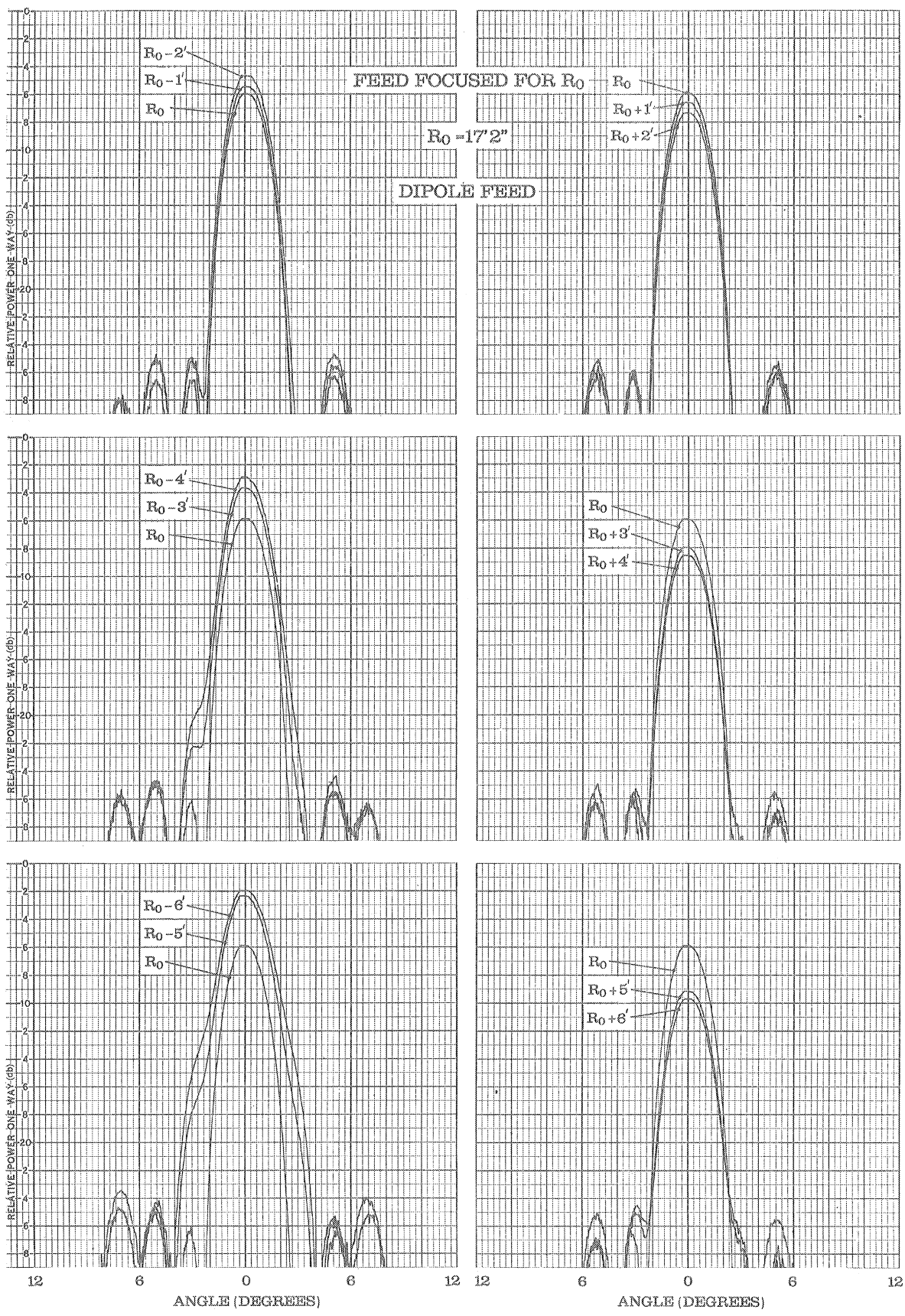
FIG. 4.9: H-PLANE NEAR FIELD PATTERNS OF ELLIPTICAL REFLECTOR
WITH DIPOLE FEED
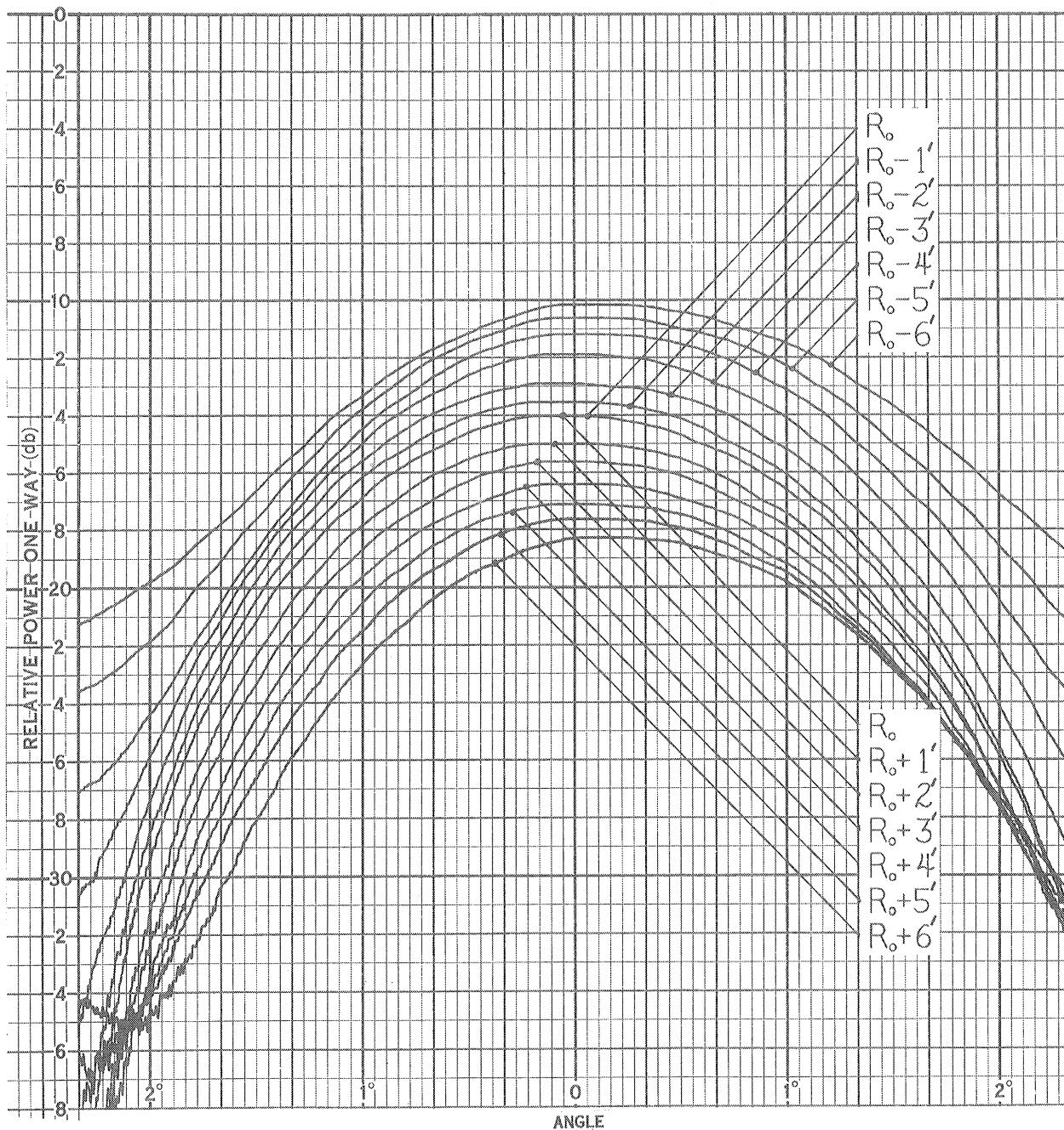
FIG. 4.10: H-PLANE NEAR FIELD PATTERNS WITH EXPANDED ANGLE SCALE, ELLIPTICAL REFLECTOR WITH DIPOLE FEED
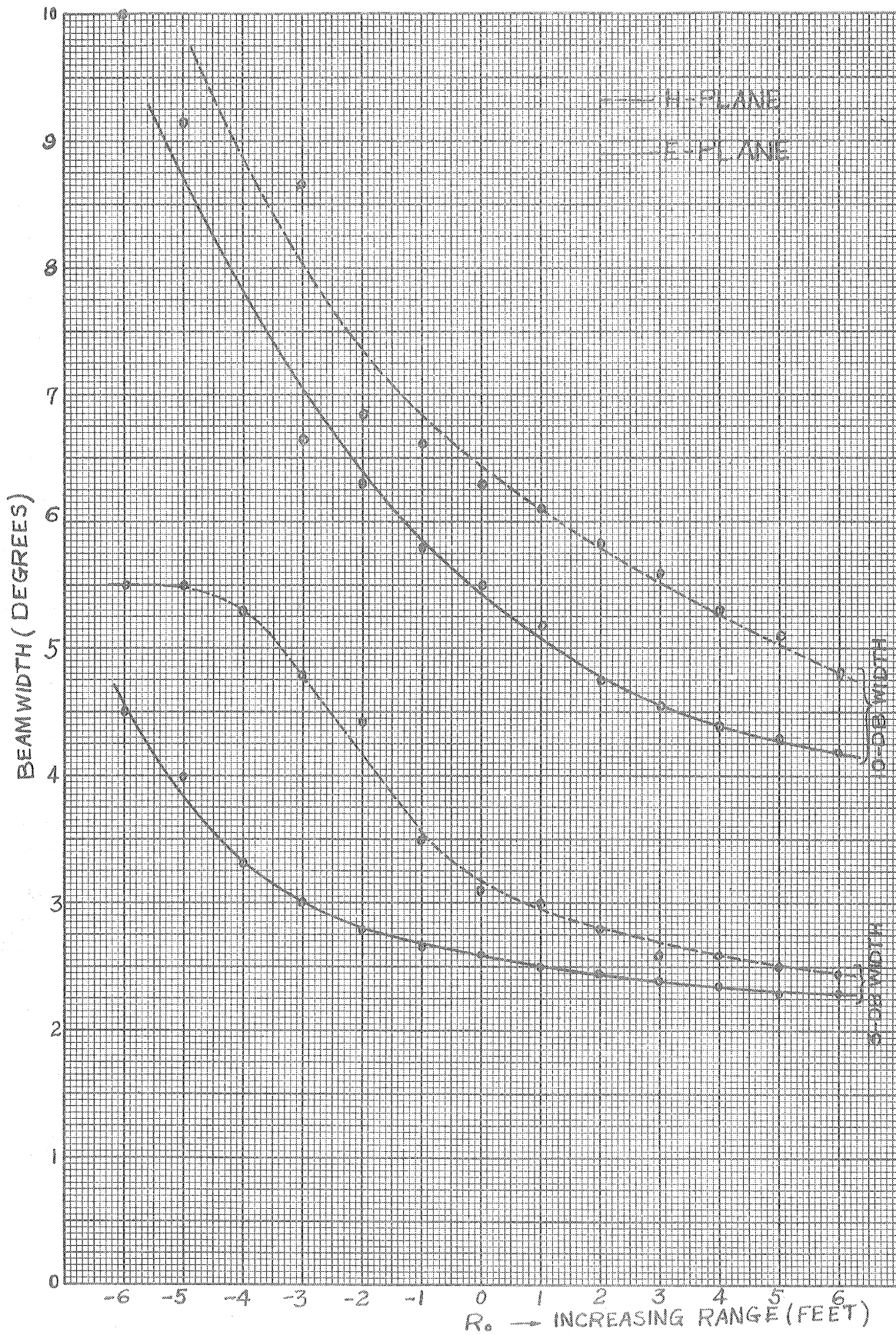
FIG. 4.11: PARABOLIC REFLECTOR FOCUSED FOR FAR FIELD,
SUMMARY OF BEAMWIDTHS VS. RANGE
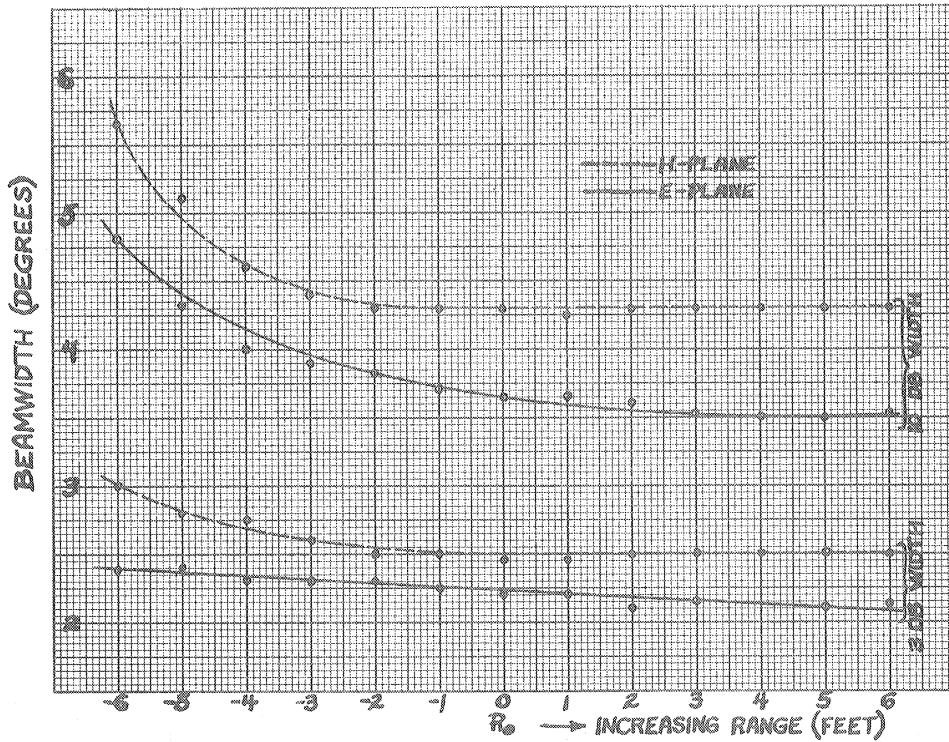
FIG. 4.12: PARABOLIC REFLECTOR FOCUSED FOR R_O,
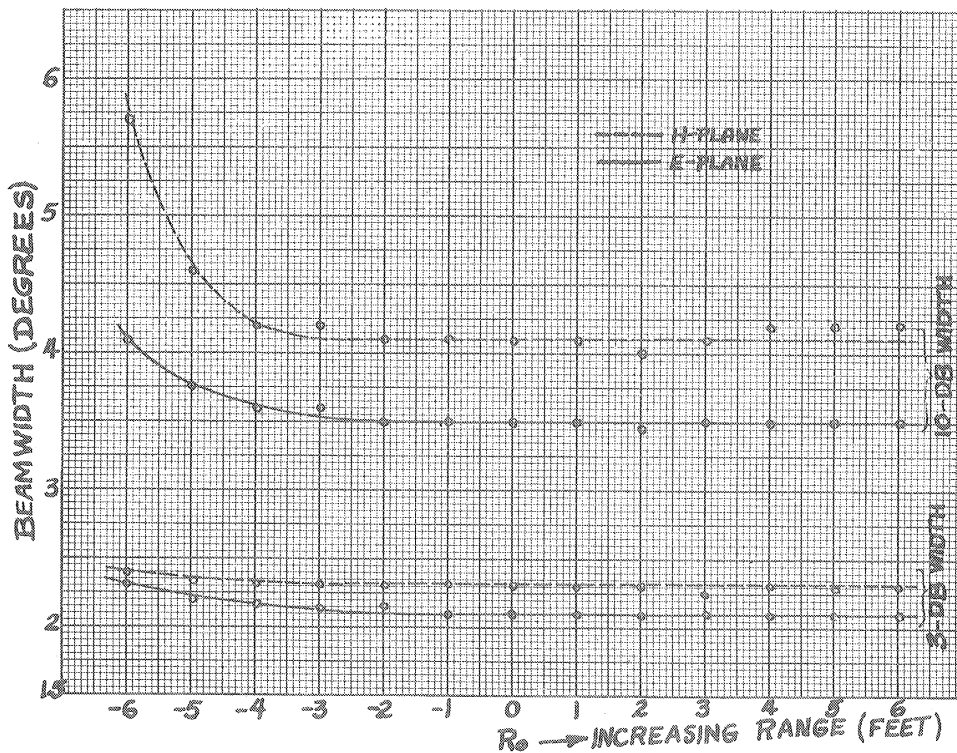SUMMARY OF BEAMWIDTHS VS. RANGE

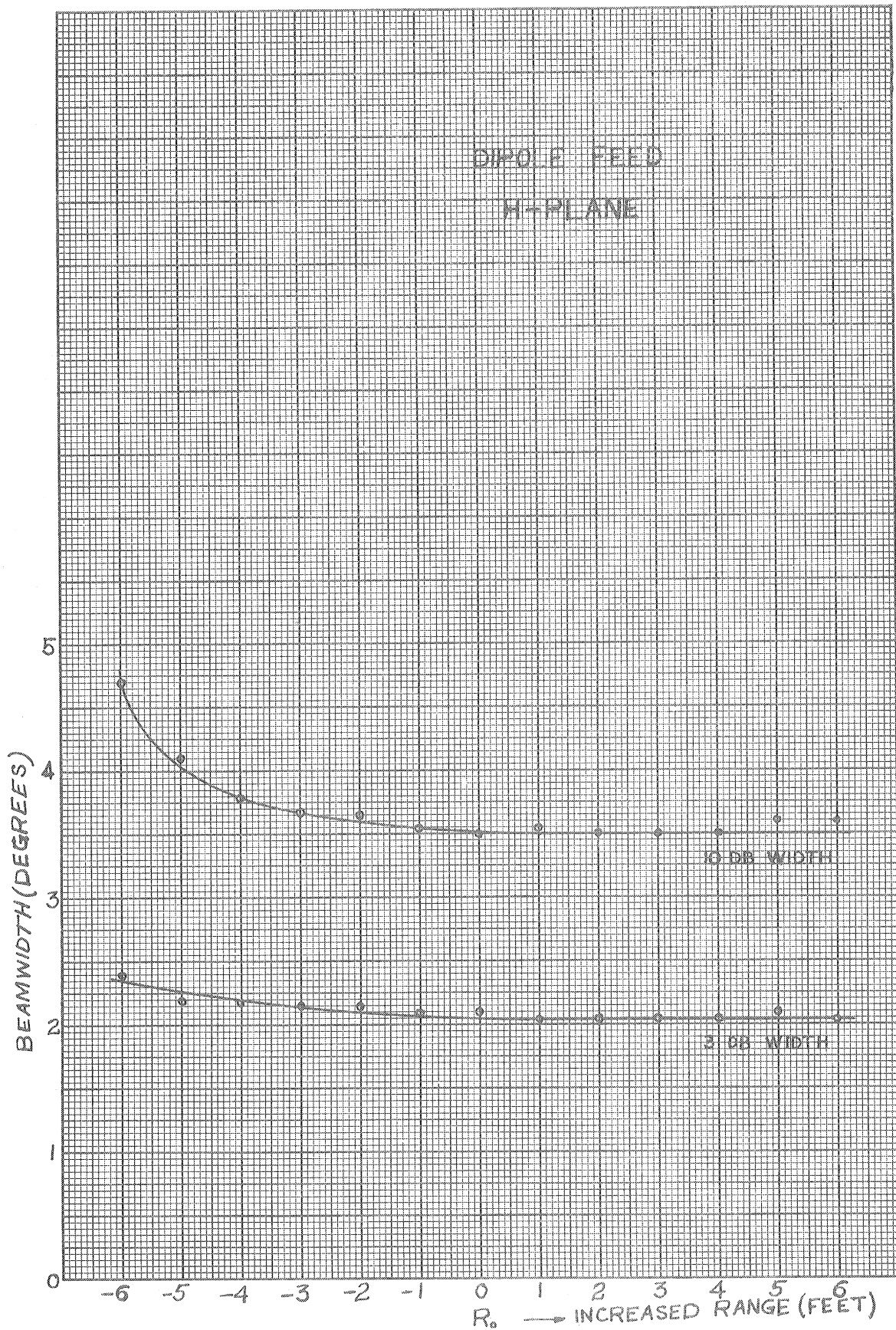FIG. 4.13: ELLIPTICAL REFLECTOR FOCUSED FOR R_O,
SUMMARY OF BEAMWIDTHS VS. RANGE

FIG. 4.14: ELLIPTICAL REFLECTOR WITH DIPOLE FEED,
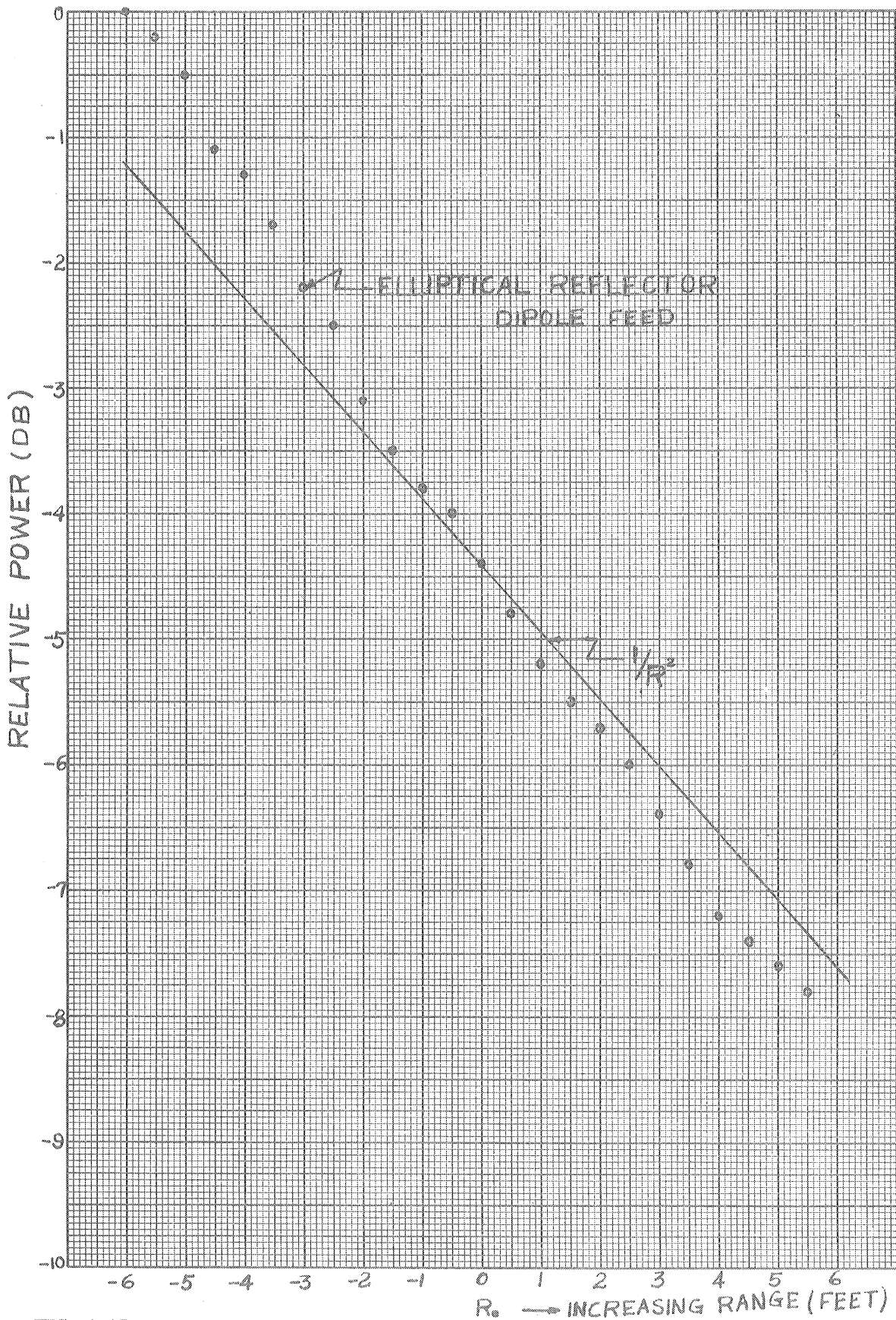SUMMARY OF BEAMWIDTHS VS. RANGE

FIG. 4.15: POWER RECEIVED VS. RANGE ON AXIS OF ELLIPTICAL REFLECTOR

48

ACKNOWLEDGEMENTS

REFERENCES

1. Watson, G. N., Theory of Bessel Functions, 2nd Edition, Cambridge at the University Press (1952).

2. Jahnke, E. and Emde, F., Tables of Functions With Formulae and Curves, Dover Publications, New York (1945).

3. Silver, S., Microwave Antenna Theory and Design, Massachusetts Institute of Technology, Radiation Laboratory Series No. 12, McGraw-Hill Book Co., Inc. (1949)

4. Bekefi, G., "Studies in Microwave Optics," E. E. R. L. Technical Report No. 38, McGill University, Montreal, Canada, (March 1957).